

# 1 Dissolved CH<sub>4</sub> coupled to Photosynthetic Picoeukaryotes in Oxic 2 Waters and to Cumulative Chlorophyll-a in Anoxic Waters of 3 Reservoirs

4 Elizabeth León-Palmero<sup>1</sup>, Alba Contreras-Ruiz<sup>1</sup>, Ana Sierra<sup>2</sup>, Rafael Morales-Baquero<sup>1</sup>, Isabel Reche<sup>1,3</sup>

5 <sup>1</sup>Instituto del Agua and Departamento de Ecología, Universidad de Granada, Granada, 18071, Spain

6 <sup>2</sup>Departamento de Química-Física and Instituto Universitario de Investigación Marina (INMAR), Facultad de Ciencias del  
7 Mar y Ambientales, Universidad de Cádiz, Puerto Real, 11510, Cádiz, Spain

8 <sup>3</sup>Research Unit Modeling Nature (MNat), Universidad de Granada, Granada, 18071, Spain

9 *Correspondence to:* Isabel Reche (ireche@ugr.es)

10

11 **Abstract.** Methane (CH<sub>4</sub>) emissions from reservoirs are responsible for most of the atmospheric climatic forcing of these  
12 aquatic ecosystems, comparable to emissions from paddies or biomass burning. Primarily, CH<sub>4</sub> is produced during the  
13 anaerobic mineralization of organic carbon in anoxic sediments by methanogenic archaea. However, the origin of the  
14 recurrent and ubiquitous CH<sub>4</sub> supersaturation in oxic waters (i.e., the methane paradox) is still controversial. Here, we  
15 determined the dissolved CH<sub>4</sub> concentration in the water column of twelve reservoirs during summer stratification and  
16 winter mixing to explore CH<sub>4</sub> sources in oxic waters. Reservoirs size ranged from 1.18 to 26.13 km<sup>2</sup>. We obtained that  
17 dissolved CH<sub>4</sub> in the water column varied up to four orders of magnitude (0.02-213.64 μM), and all oxic depths were  
18 consistently supersaturated in both periods. Phytoplanktonic sources appear to determine the concentration of CH<sub>4</sub> in these  
19 reservoirs primarily. In anoxic waters, the depth-cumulative chlorophyll-a concentration, a proxy for the phytoplanktonic  
20 biomass exported to sediments, was correlated to CH<sub>4</sub> concentration. In oxic waters, the photosynthetic picoeukaryotes  
21 abundance was significantly correlated to the dissolved CH<sub>4</sub> concentration both during the stratification and the mixing. The  
22 mean depth of the reservoirs, as a surrogate of the vertical CH<sub>4</sub> transport from sediment to the oxic waters, also contributed  
23 notably to the CH<sub>4</sub> concentration in oxic waters. Our findings suggest that photosynthetic picoeukaryotes can have a  
24 significant role in determining CH<sub>4</sub> concentration in oxic waters, although their role as CH<sub>4</sub> sources to explain methane  
25 paradox has been poorly explored.

## 26 1 Introduction

27 Lakes and reservoirs are significant sources of methane (CH<sub>4</sub>), affecting the atmospheric climatic forcing (Deemer et al.,  
28 2016). The estimated contribution of lakes to global emission budget is ca. 71.6 Tg CH<sub>4</sub> year<sup>-1</sup> (Bastviken et al., 2011), and

29 the specific contribution of reservoirs ranges between 4 and 70 Tg CH<sub>4</sub> year<sup>-1</sup>, representing up to 10 % of total CH<sub>4</sub>  
30 emissions (Deemer et al., 2016). Although freshwaters only cover about 5-8 % of the Earth's surface (Mitsch et al., 2012),  
31 they emit more CH<sub>4</sub> than the ocean surface (Saunois et al., 2016). Traditionally, the net CH<sub>4</sub> production is determined by  
32 archaeal methanogenesis, which produces methane as an end product of organic matter degradation in anoxic conditions, and  
33 to methanotrophs, which consume it in oxic conditions (Schubert and Wehrli, 2018). In freshwater ecosystems, the anoxic  
34 sediments are a primary source of CH<sub>4</sub> (Segers, 1998), where methanogens are very sensitive to temperature and quantity  
35 and quality of the organic matter used as substrate (Marotta et al., 2014; Rasilo et al., 2015; Sepulveda-Jauregui et al., 2018;  
36 Thanh-Duc et al., 2010; West et al., 2012; Yvon-Durocher et al., 2014). They are also affected by the extent of anoxia in the  
37 sediments, as far as they are obligate anaerobes and will not survive and produce CH<sub>4</sub> under aerobic conditions  
38 (Chistoserdova et al., 1998; Schubert and Wehrli, 2018). However, many observations from freshwaters and marine waters  
39 have detected CH<sub>4</sub> supersaturation in the oxic layers. A widespread phenomenon described as the "methane paradox"  
40 (Bogard et al., 2014; Damm et al., 2010; Donis et al., 2017; Grossart et al., 2011; Kiene, 1991; Murase et al., 2003; Owens et  
41 al., 1991; Schmidt and Conrad, 1993; Schulz et al., 2001; Tang et al., 2014, 2016).

42 This persistent CH<sub>4</sub> supersaturation in oxic layers of marine and freshwater ecosystems requires extra inputs to  
43 compensate for the CH<sub>4</sub> losses by methanotrophy and the emissions toward the atmosphere. CH<sub>4</sub> inputs may come from  
44 anoxic sediments or from *in situ* sources in the oxic layers. The transport of CH<sub>4</sub> from the bottom and littoral sediments in  
45 shallow zones has been proposed to explain the supersaturation in the surface waters of some lakes (Bastviken et al., 2004;  
46 Encinas Fernández et al., 2016; Michmerhuizen et al., 1996; Murase et al., 2003; Peeters et al., 2019; Rudd and Hamilton,  
47 1978). The vertical transport may be relevant in small lakes, but in deep and thermally stratified systems, the vertical  
48 diffusion rates of dissolved gases across the thermocline are too low, and there is not apparent CH<sub>4</sub> upward movements from  
49 the hypolimnion (Peeters et al., 1996; Rudd and Hamilton, 1978). In fact, Thalasso et al. (2020) determined that there was no  
50 exchange between the hypolimnion and the epilimnion in a Siberian lake. The CH<sub>4</sub> produced in the sediments and the  
51 hypolimnion was assimilated there. Consequently, the CH<sub>4</sub> in the epilimnion came from lateral transport and *in situ*  
52 production. Lateral CH<sub>4</sub> transport from shallow sediments of the littoral zones may be a significant source in the open  
53 surface of some lakes and reservoirs. DelSontro et al. (2018) resolved that CH<sub>4</sub> transport from littoral zones was relevant for  
54 the dissolved CH<sub>4</sub> in the epilimnion of small lakes. However, lateral transport does not fully explain CH<sub>4</sub> supersaturation in  
55 the open ocean, and large freshwater ecosystems, hence, other *in situ* CH<sub>4</sub> sources likely occur (Damm et al., 2010;  
56 DelSontro et al., 2018; Grossart et al., 2011; Khatun et al., 2020; Owens et al., 1991; Schmidt and Conrad, 1993; Schulz et  
57 al., 2001; Scranton and Brewer, 1977; Tang et al., 2014; Tilbrook and Karl, 1995).

58 Previous works demonstrated the *in situ* CH<sub>4</sub> production in oxic waters using stable isotope techniques in  
59 experiments, mesocosms, and field samples (Bižić et al., 2020; Bogard et al., 2014; DelSontro et al., 2018; Hartmann et al.,  
60 2020; Tang et al., 2016) and using molecular approaches (Grossart et al., 2011; Khatun et al., 2020; Yao et al., 2016a). In the  
61 literature, there are different alternatives proposed as CH<sub>4</sub> sources. On the one hand, the occurrence of methanogenesis in  
62 micro-anoxic niches in the guts of zooplankton, and within sinking particles (Angelis and Lee, 1994; Karl and Tilbrook,

63 1994). In both micro-niches, the CH<sub>4</sub> production appeared to be too low to sustain the total CH<sub>4</sub> supersaturation of the oxic  
64 waters (Schmale et al., 2018; Tang et al., 2014). On the other hand, there is a consistent link between dissolved CH<sub>4</sub>  
65 concentration and autotrophic organisms, primary production, and chlorophyll-a concentration (Bogard et al., 2014; Grossart  
66 et al., 2011; Owens et al., 1991; Schmidt and Conrad, 1993; Tang et al., 2014). Grossart et al., (2011) detected potential  
67 methanogenic *Archaea* attached to photoautotrophs as *Chlorophyta* (*Eukarya*) and *Cyanobacteria* (*Bacteria*) in the  
68 epilimnion of an oligotrophic lake and confirmed the production of CH<sub>4</sub> in the presence of oxygen in laboratory incubations.  
69 If occurring, that symbiosis would require that the methanogenic microorganisms tolerate the oxygen exposure as it has been  
70 observed by several authors (Angel et al. 2011; Angle et al., 2017; Jarrell, 1985), in contrast to general belief. New findings  
71 suggest that the link between phytoplankton and dissolved CH<sub>4</sub> may rely on diverse metabolic pathways in *Bacteria* and  
72 *Eukarya*. These metabolic pathways contribute to the dissolved CH<sub>4</sub> in oxic waters due to the degradation of methylated  
73 compounds. In the open ocean, archaea and bacteria appear to metabolize the algal osmolyte dimethylsulfoniopropionate  
74 producing methane as a by-product (Damm et al., 2008, 2010, 2015; Zindler et al., 2013). Common methyl-containing  
75 substances as methionine produce methane in algae, saprotrophic fungi, and plants (Lenhart et al., 2012, 2015, 2016).  
76 Another reported pathway is the degradation of methyl-phosphonates (MPn) as an alternative source of phosphorus (P) in  
77 phosphate-starved bacterioplankton. The hydrolysis of these compounds, using the enzyme C–P lyase, also releases methane  
78 as a by-product. This pathway appears in chronically P starved ecosystems as the ocean gyres, oligotrophic lakes, and  
79 microbial mats (Beversdorf et al., 2010; Carini et al., 2014; Gomez-Garcia et al., 2011; Karl et al., 2008; Repeta et al., 2016;  
80 Teikari et al., 2018; del Valle and Karl, 2014; Wang et al., 2017; Yao et al., 2016a). Recent studies using phytoplankton  
81 cultures and stable isotope techniques propose that the production of CH<sub>4</sub> may rely directly on the photoautotrophic carbon  
82 fixation of algae and *Cyanobacteria* (Bižić et al., 2020; Hartmann et al., 2020; Klintzsch et al., 2019; Lenhart et al., 2016).  
83 These sources of CH<sub>4</sub> in oxic waters, however, still have not been tested simultaneously in reservoirs, despite the known  
84 high contribution of these freshwater ecosystems to global CH<sub>4</sub> emissions.

85 In this study, we measured the dissolved CH<sub>4</sub> concentration in the water column of twelve reservoirs that cover a  
86 broad spectrum of sizes, ages, morphometries, and trophic states during the summer stratification and winter mixing (León-  
87 Palmero et al., 2020). Our objective was to assess the relative contribution of different sources of CH<sub>4</sub> in the oxic waters and  
88 to shed light on the methane paradox depending on reservoir properties. We explored the following CH<sub>4</sub> sources in oxic  
89 waters: 1) vertical and lateral transport of CH<sub>4</sub> from hypolimnetic and littoral waters; 2) *in situ* production by methanogenic  
90 *Archaea* tolerant to oxygen; 3) *in situ* production by methylphosphonate degradation; 4) *in situ* production by photosynthetic  
91 microorganisms. We used the concentration chlorophyll-a, the primary productivity and the abundance of photosynthetic  
92 picoeukaryotes and cyanobacteria as variables for the photosynthetic signatures. The photosynthetic picoeukaryotes are a  
93 relevant part of the freshwater phytoplankton, but their role in the methane paradox has been particularly little studied.

## 94 2 Methods

### 95 2.1 Study Reservoirs, Morphometry, and Vertical Profiles

96 We sampled twelve reservoirs located in the southern Spain (Figure 1) between July 2016 and August 2017 once during the  
97 summer stratification and once during winter mixing. In Table 1, we show the geographical coordinates, age, and the  
98 morphometry description of the study reservoirs. The reservoirs were built between 1932 and 2003, for water supply and  
99 agriculture irrigation, and they are located in watersheds with different lithology and land-use (more details can be found in  
100 León-Palmero et al. 2019, 2020). These reservoirs differ in morphometric, chemical, and trophic characteristics covering a  
101 wide range of concentrations of dissolved organic carbon (DOC), total nitrogen (TN), total phosphorus (TP), and  
102 chlorophyll-a (Table 2). All raw data for the water column was deposited in Pangaea database  
103 (<https://doi.org/10.1594/PANGAEA.912535>).

104 We obtained the reservoir surface area, perimeter, and volume using the following open databases: Infraestructura  
105 de Datos Espaciales de Andalucía (IDEAndalucía; <http://www.ideandalucia.es/portal/web/ideandalucia/>), and the Ministerio  
106 para la Transición Ecológica (<https://www.embalses.net/>).

107 The mean depth was calculated as follows (Eq. 1):

$$108 \text{ Mean depth (m)} = \frac{\text{Volume (m}^3\text{)}}{\text{Surface area (m}^2\text{)}} \quad (1)$$

109 The shoreline development ratio ( $D_L$ ) (Aronow, 1982) is a comparative index relating the shoreline length (i.e., the perimeter  
110 of the reservoir) to the circumference of a circle that has the same area. The closer this ratio is to 1, the more circular the  
111 lake. A large ratio ( $\gg 1$ ) indicates the shoreline is more scalloped than a low ratio. The equation is as follows (Eq. 2):

$$112 D_L = \frac{\text{Length of the shoreline (m)}}{2\sqrt{\pi \text{ Area (m}^2\text{)}}}, \quad (2)$$

113 The shallowness index ( $m^{-1}$ ) was obtained by dividing the shoreline development index ( $D_L$ ) by the mean depth (m), as  
114 follows in eq. 3:

$$115 \text{ Shallowness index (m}^{-1}\text{)} = \frac{D_L}{\text{Mean depth (m)}} \quad (3)$$

116 We sampled the water column near the dam, in the open waters of the reservoir. During the stratification and the  
117 mixing period, we selected the same location. First, we performed a vertical profile of the reservoir using a Seabird 19plus  
118 CTD profiler, coupled to Spherical Underwater Quantum Sensor (LI-193R), and a fluorimeter Turner® SCUFA (model  
119 CYCLOPS-7) for continuous measurements of temperature ( $^{\circ}\text{C}$ ), dissolved oxygen ( $\mu\text{M}$ ), conductivity ( $\mu\text{S/cm}$ ), turbidity  
120 (FTU), density ( $\text{kg m}^{-3}$ ), photosynthetic active radiation, chlorophyll-a fluorescence ( $\mu\text{g L}^{-1}$ ), specific conductance ( $\mu\text{S/cm}$ ),  
121 and salinity (psu). Then, based on the temperature and oxygen profiles, we selected from 6 to 9 depths representative of the  
122 oxic, anoxic layers, and the transition between them in the different reservoirs. We took the water samples using a UWITEC  
123 sampling bottle of 5 liters with a self-closing mechanism. We collected samples for the dissolved  $\text{CH}_4$  analysis in 125 or 250  
124 mL air-tight Winkler bottles by duplicate (250 mL) or triplicate (125 mL). We filled up the bottles very carefully from the  
125 bottom to avoid the formation of bubbles and minimize the loss of  $\text{CH}_4$  during field sampling. We preserved the samples

126 with a solution of  $\text{HgCl}_2$  (final concentration 1mM) to inhibit biological activity and sealed the bottles with Apiezon® grease  
127 to prevent gas exchanges. We also took samples from each depth to the chemical and biological analysis explained below.  
128 We also measured barometric pressure using a multi-parameter probe (HANNA HI 9828) for the gas saturation calculations.  
129 We calculated the saturation values (%) for dissolved oxygen as the ratio of the dissolved gas measured and the gas  
130 concentration expected in equilibrium. We calculated the gas concentration in equilibrium, taking into account the  
131 differences in temperature, salinity, and barometric pressure (Mortimer, 1956).

## 132 **2.2 Dissolved $\text{CH}_4$ in the water column**

133 We stored the Winkler bottles in the dark at room temperature until analysis in the laboratory. We measured dissolved  $\text{CH}_4$   
134 using headspace equilibration in a 50 ml air-tight glass syringe (Agilent P/N 5190–1547) (Sierra et al., 2017). We obtained  
135 two replicates for each 150 mL Winkler bottle, and three replicates for each 250 mL Winkler bottle. We took a quantity of  
136 25 g of water ( $\pm 0.01$  g) using the air-tight syringe and added a quantity of 25 mL of a standard gas mixture that had a  
137 methane concentration similar to atmospheric values (1.8 ppmv) to complete the volume of the syringe. The syringes were  
138 shaken for 5 min (VIBROMATIC Selecta) to ensure mixing, and we waited 5 min to reach complete equilibrium. Then, the  
139 gas in the syringe was injected manually in the gas chromatograph (GC; Bruker® GC-450) equipped with Hydrogen Flame  
140 Ionization Detector (FID). We daily calibrated the detectors using three standard gas mixtures with  $\text{CH}_4$  mixing ratios of  
141 1952, 10064, 103829 ppbv, made and certified by Air Liquide (France). We calculated the gas concentration in the water  
142 samples from the concentration measured in the headspace using the Bunsen functions for  $\text{CH}_4$  (Yamamoto *et al* 1976,  
143 Wiesenburg and Guinasso 1979). The precision in the quantification of the gas mixture of  $\text{CH}_4$  used in the headspace  
144 equilibrium (1.8 ppmv) expressed as the coefficient of variation was 3.7% ( $n = 123$ ). The precision of the measurement of  
145 the dissolved  $\text{CH}_4$  concentration, that included the analytical processing of the samples and the equilibration step, was 3.6%  
146 for four to six replicates of each sample. We calculated the saturation values (%) as the ratio between the concentration of  
147 the dissolved gas measured and the gas concentration expected in equilibrium considering the temperature, salinity, and  
148 barometric pressure of each reservoir. We used the atmospheric gas concentrations provided by *The Global Greenhouse Gas*  
149 *Reference Network* website (<https://www.esrl.noaa.gov/gmd/ccgg/index.html>), which is part of the National Oceanic and  
150 Atmospheric Administration (NOAA) Earth System Research Laboratory in Boulder, Colorado. We calculated the 2016  
151 global mean atmospheric concentrations for  $\text{CH}_4$  (Dlugokencky, 2019) from the 2016 global monthly mean. The differences  
152 among these values and the local atmospheric concentrations are assumed to be small compared with the high dissolved  
153 concentrations obtained in the study reservoirs.

## 154 **2.3 Chemical analysis in the water column**

155 From the discrete sampling, we selected 3 or 4 representative depths of the epilimnion, metalimnion (oxycline), and  
156 hypolimnion/bottom layers for nutrient analysis during the stratification period. We also selected 3 or 4 equivalent depths  
157 during the mixing period. In total, we analyzed 77 samples: 41 samples from the stratification period, and 36 samples from

158 the mixing period. We determined total nutrients using unfiltered water, while we filtered the samples through pre-  
159 combusted 0.7- $\mu\text{m}$  pore-size Whatman GF/F glass-fiber filters for the dissolved nutrients. We acidified the samples for  
160 dissolved organic carbon (DOC), total dissolved nitrogen (TDN), and total nitrogen (TN) samples with phosphoric acid  
161 (final  $\text{pH} < 2$ ). We measured DOC, TN, and TDN by high-temperature catalytic oxidation using a Shimadzu total organic  
162 carbon (TOC) analyzer (Model TOC-V CSH) coupled to a nitrogen analyzer (TNM-1). We calibrated the instrument using a  
163 four-point standard curve of dried potassium hydrogen phthalate for DOC, and dried potassium nitrate for TN and TDN  
164 (Álvarez-Salgado and Miller, 1998). We analyzed two replicates and three to five injections per replicate for each sample.  
165 We purged the DOC samples with phosphoric acid for 20 min to eliminate all the dissolved inorganic carbon. The precision  
166 of the DOC measurements expressed as the mean coefficient of variation was 3.0%. The mean precision for the TN and  
167 TDN was 8.2% and 2.9%, respectively.

168 We measured the  $\text{NO}_3^-$  concentration by duplicate using the ultraviolet spectrophotometric method, using a Perkin  
169 Elmer UV-Lambda 40 spectrophotometer at wavelengths of 220 nm and correcting for DOC absorbance at 275 nm (Baird et  
170 al., 2012). The mean coefficient of variation was 0.5%. We measured  $\text{NH}_4^+$  and  $\text{NO}_2^-$  concentrations by Inductively Coupled  
171 Plasma Optical Emission Spectrometry (ICP-OES). Dissolved inorganic nitrogen (DIN) was calculated as the addition of the  
172  $\text{NO}_3^-$ ,  $\text{NH}_4^+$ , and  $\text{NO}_2^-$  concentrations. The detection limit for the  $\text{NH}_4^+$ , and  $\text{NO}_2^-$  concentrations were 3.6  $\mu\text{M}$  and 1.4  $\mu\text{M}$ ,  
173 respectively. We measured total phosphorus (TP) concentration by triplicate using the molybdenum blue method (Murphy  
174 and Riley, 1962) after digestion with a mixture of potassium persulphate and boric acid at 120  $^\circ\text{C}$  for 30 min (Baird et al.,  
175 2012). The precision in the quantification of the TP concentration was 11.1%.

#### 176 **2.4 Chlorophyll-a, Phytoplankton, and Primary Production in the water column**

177 We determined the chlorophyll-*a* concentration, and the abundances of cyanobacteria and photosynthetic picoeukaryotes in  
178 all the depths sampled during the discrete samplings ( $n = 178$ ). We determined the chlorophyll-*a* concentration by filtering  
179 the particulate material of 500 to 2000 ml of water through pre-combusted Whatman GF/F glass-fiber filters. Then, we  
180 extracted the pigments from the filters with 95% methanol in the dark at 4  $^\circ\text{C}$  for 24 h (Baird et al., 2012). We measured  
181 chlorophyll-*a* (Chl-*a*) absorption using a Perkin Elmer UV-Lambda 40 spectrophotometer at the wavelength of 665 nm and  
182 for scattering correction at 750 nm. The detection limit was 0.1  $\mu\text{g L}^{-1}$ .

183 To obtain the cumulative chlorophyll-*a* in the whole water column ( $\text{mg Chl-}a \text{ m}^{-2}$ ), from the discrete depths, we  
184 summed the concentration of Chl-*a* from each stratum using the trapezoidal rule (León-Palmero et al., 2019), as indicated in  
185 the following equation (4):

$$186 \text{ Cumulative Chl-}a = \sum_{k=1}^n X_{ik} * (Z_{k+1} - \frac{Z_{k-1}}{2}) \quad (4)$$

187 Where  $Z$  stands for the depth considered, and  $n$  is the number of depths sampled.  $Z_k$  stands for the  $n$  sampled depth;  $X_{ij}$  is the  
188 Chl-*a* concentration ( $\mu\text{g L}^{-1}$ ) at the depth  $Z_k$ .

189 We determined by triplicate the abundances of cyanobacteria and photosynthetic picoeukaryotes using flow cytometry using  
 190 unfiltered water. We collected and fixed the samples with a mixture of 1% paraformaldehyde and 0.05% glutaraldehyde for  
 191 30 min in the dark at 4 °C. Then, we froze the samples in liquid nitrogen and stored them at -80 °C until analysis. We  
 192 analyzed the samples in the FACScalibur flow cytometer equipped with the BD CellQuest Pro software for data analysis.  
 193 We used yellow-green 0.92 µm latex beads (Polysciences) as an internal standard to control the cytometer performance  
 194 every day. We used different signals for groups determination: the side scatter (SSC), chlorophyll-a (red fluorescence, FL3),  
 195 phycoerythrin (the orange fluorescence, FL2), and phycocyanin (the blue fluorescence, FL4); following the protocols and  
 196 indications for data analysis of previous works (Cellamare et al., 2010; Collier, 2000; Corzo et al., 1999; Gasol and Giorgio,  
 197 2000; Liu et al., 2014). In figure S13, we show a cytogram of the populations of cyanobacteria and photosynthetic  
 198 picoeukaryotes. The mean coefficient of variation for the abundances of cyanobacteria and photosynthetic picoeukaryotes  
 199 was 8.8% and 11.4%, respectively.

200 We estimated gross primary production (GPP), net ecosystem production (NEP), and ecosystem respiration (R) by  
 201 measuring temporal changes in dissolved oxygen concentration and temperature using a miniDOT (PME) submersible water  
 202 logger during the stratification period. We recorded measurements every 10 minutes for 24-48 hours during the same  
 203 sampling days. Briefly, the equation for estimating free-water metabolism from measurements of dissolved oxygen was  
 204 established by Odum (1956) (equation 5):

$$205 \Delta O_2 / \Delta t = GPP - R - F - A \quad (5)$$

206 Where  $\Delta O_2 / \Delta t$  is the change in dissolved oxygen concentration through time; F is the exchange of  $O_2$  with the atmosphere;  
 207 and A is a term that combines all other processes that may cause changes in the dissolved oxygen concentration as horizontal  
 208 or vertical advection, and it is often assumed to be negligible. The calculations were performed as in Staehr et al., (2010).  
 209 The physical gas flux was modelled as follows (equation 6):

$$210 F \left( g O_2 m^{-2} h^{-1} \right) = k \left( O_{2 \text{ meas}} - O_{2 \text{ sat}} \right) \quad (6)$$

211 Where F is the physical gas flux,  $k \left( m h^{-1} \right)$  is the piston velocity estimated following the equation of Jähne et al., (1987) and  
 212 the indications of Staehr et al., (2010).  $O_{2 \text{ meas}}$  is the actual oxygen concentration ( $mg mL^{-1}$ ), and  $O_{2 \text{ sat}}$  is the oxygen  
 213 concentration in water in equilibrium with the atmosphere at ambient temperature and salinity.

214 We calculated the hourly net ecosystem production ( $NEP_{hr}$ ) and the daytime net ecosystem production ( $NEP_{daytime}$ )  
 215 following the equations 7 (Cole et al., 2000) and 8:

$$216 NEP_{hr} \left( g O_2 m^{-3} h^{-1} \right) = \Delta O_2 \left( g m^{-3} h^{-1} \right) - F / Z_{mix} \quad (7)$$

$$217 NEP_{daytime} \left( g O_2 m^{-3} \text{ daylight period}^{-1} \right) = \text{mean } NEP_{hr} \text{ during daylight} \left( g O_2 m^{-3} h^{-1} \right) \times \text{Light hours (h)} \quad (8)$$

218  $NEP_{hr}$  is directly derived from the changes in dissolved oxygen ( $\Delta O_2$ ), after accounting for physical gas flux with the  
 219 atmosphere (F).  $Z_{mix}$  is the depth of the mixed layer (m), and that was inferred from the temperature profile as the upper  
 220 mixed zone where the temperature remains constant.  $NEP_{daytime}$  is the portion of NEP between sunrise and sunset, when the

221 photosynthesis is taking place. We obtained the exact light hours from an online solar calculator  
 222 (<https://es.calcuworld.com/calendarios/calcular-salida-y-puesta-del-sol/>). We established the start and the end time for  
 223 photosynthesis as 30 minutes before sunrise and 30 minutes after dawn (Schlesinger and Bernhardt, 2013). We obtained  
 224 hourly R ( $R_{hr}$ ), R during the daytime ( $R_{daytime}$ ), and R during all the day ( $R_{day}$ ) following equation 9, 10, and 11,  
 225 respectively:

$$226 R_{hr} \left( g O_2 m^{-3} h^{-1} \right) = \text{mean } NEP_{hr} \text{ during darkness } \left( g O_2 m^{-3} h^{-1} \right) \quad (9)$$

$$227 R_{daytime} \left( g O_2 m^{-3} \text{ daylight period}^{-1} \right) = R_{hr} \left( g O_2 m^{-3} h^{-1} \right) \times \text{Light hours (h)} \quad (10)$$

$$228 R_{day} \left( g O_2 m^{-3} d^{-1} \right) = R_{hr} \left( g O_2 m^{-3} h^{-1} \right) \times 24 \text{ (h)} \quad (11)$$

229 We calculated the respiration rate during the night (the period between 60 minutes after dawn and 60 minutes before sunrise)  
 230 (Staehr et al., 2010), and we assumed that the respiration rate overnight was similar to the respiration rate over the day.  
 231 Finally, we obtained the GPP and NEP for the day (equation 12 and 13):

$$232 GPP \left( g O_2 m^{-3} d^{-1} \right) = NEP_{daytime} + R_{daytime} \quad (12)$$

$$233 NEP \left( g O_2 m^{-3} d^{-1} \right) = GPP - R_{day} \quad (13)$$

## 234 2.5 DNA analysis

235 We selected 3 or 4 representative depths for determining the abundance of the functional genes of the epilimnion,  
 236 metalimnion (oxycline), and hypolimnion/bottom layers during the stratification period. We also selected 3 or 4 equivalent  
 237 depths during the mixing period. In total, we analyzed 41 samples from the stratification period and 36 samples for the  
 238 mixing period. We pre-filtered the water through 3.0  $\mu m$  pore-size filters and extracted DNA following the procedure  
 239 developed by Boström et al., (2004) for environmental samples. During the DNA extraction protocol, we combined a cell  
 240 recovery step by centrifugation of 12 - 20 mL of the pre-filtered water, a cell lysis step with enzyme treatment (lysozyme and  
 241 proteinase K), and finally, the DNA recovery step with a co-precipitant (yeast tRNA) to improve the precipitation of low-  
 242 concentration DNA. DNA was quantified using a DNA quantitation kit (Sigma-Aldrich) based on the fluorescent dye  
 243 bisBenzimide (Hoechst 33258). Extracted DNA served as the template for PCR and quantitative PCR (qPCR) analysis to test  
 244 the presence and abundance of the *mcrA* gene and the *phnJ* gene. For PCR analysis, we used the recombinant Taq DNA  
 245 Polymerase (Thermo Fisher Scientific) using the Mastercycler X50 thermal cycler (Eppendorf). We ran the qPCR plates  
 246 using SYBR Green as the reporter dye (PowerUp™ SYBR™ Green Master Mix, Thermo Fisher Scientific) in the Applied  
 247 Biosystems 7500 Real-Time PCR System and the 7500 Software. In both cases, PCR and qPCR, we designed the standard  
 248 reaction mix recipes and the thermocycling conditions using the provider specifications and primer requirements. We chose  
 249 specific primers from studies performed in natural samples of freshwaters. We used pure cultures as positive controls (more  
 250 details below).



251 We targeted the alpha subunit of methyl-coenzyme reductase (*mcrA*) as a genetic marker to determine the existence and  
252 abundance of methanogenic *Archaea* in our samples. This gene appears to be an excellent marker since all known  
253 methanogens have the *methyl coenzyme-M reductase*, which is the enzyme responsible for the conversion of a methyl group  
254 to CH<sub>4</sub> (Grabarse et al., 2001). We used specific primers from West et al. (2012) adapting their procedure. The forward  
255 primer was mcrAqF (5'-AYGGTATGGARCAGTACGA-3'), and the reverse primer was mcrAqR (5'-  
256 TGVAGRTC GTABCCGWAGAA -3'), and the annealing temperature was 54 °C. The expected size of the PCR product was  
257 ~200 bp. We used a culture of *Methanosarcina acetivorans* (ATCC 35395) as a positive control. We tested all the samples  
258 (n=77). We also tested the presence of the *phnJ* gene, which encodes a subunit of the C-P lyase complex (Seweryn et al.,  
259 2015; White and Metcalf, 2007). This enzyme cleaves C-P bonds in phosphonate compounds releasing methane, and  
260 changes in response to the phosphate availability (Yao et al., 2016a). We ran the amplification with a pair of primers  
261 previously used by Fox et al., (2014); and Yao et al., (2016a). The forward primer was PhnJoc1 (5'-  
262 AARGTRATMGAYCARGG-3') and the reverse PhnJoc2 (5'-CATYTTYGGATTRTCRAA-3') adapting the PCR  
263 procedure from Yao et al., (2016a). The annealing temperature was 52.5 °C, and the positive controls were run using a pure  
264 culture of *Rhodopseudomonas palustris* (ATCC 33872). The expected size of the PCR product was ~400 bp. We checked  
265 the result of the amplification by running 1.5 % (w/v) agarose gel electrophoresis. If we did not detect amplification in the  
266 PCR or qPCR samples, we changed the standard procedure by increasing the DNA amount and the primers concentration to  
267 corroborate the negative results. We tested all the samples (n=77).

## 268 2. 6. Statistical tests

269 We conducted all the statistical analysis in R (R Core Team, 2014) using the packages car (Fox and Weisberg, 2011), nortest  
270 (Gross and Ligges, 2015), and mgcv (Wood, 2011). We performed the Shapiro-Wilk test of normality analysis and Levene's  
271 test for homogeneity of variance across groups. We performed a one-way analysis of variance test (ANOVA) when the data  
272 were normally distributed. In case the data did not meet the assumptions of normality, we used the paired Kruskal-Wallis  
273 rank-sum (K-W) or Wilcoxon (V) tests. We analyzed the potential sources of dissolved CH<sub>4</sub> using simple regression analysis  
274 and generalized additive models (GAMs) (Wood, 2006). GAM is a generalized model with a linear predictor involving a  
275 sum of smooth functions of covariates (Hastie and Tibshirani, 1986, 1990). The model structure is shown in Eq. (4):

$$276 y_i = f_1(x_{1i}) + f_2(x_{2i}) + \dots + f_n(x_{ni}) + \epsilon_i, \quad (4)$$

277 Where the  $f_j$  are the smooth functions, and the  $\epsilon_i$  are independent identically distributed  $N(0, \sigma^2)$  random variables. We fit  
278 smoothing functions by penalized cubic regression splines. The cross-validation method (Generalized Cross Validation  
279 criterion, GCV) estimates the smoothness of the functions. We fitted the models to minimize the Akaike Information  
280 Criterion (AIC) and the GCV values. We calculated the percentage of variance explained by the model (adj R<sup>2</sup>) and the  
281 quality of the fit (deviance explained). We also fixed the effect of each predictor to assess the contribution of the other

282 predictor on the total deviance explained. Then, the sum of the deviance explained by two predictors can be different from  
283 the deviance explained by the model due to interactive effects.

## 284 **3 Results and discussion**

### 285 **3.1. Profiles description**

286 We found pronounced differences in the concentration of dissolved CH<sub>4</sub> of the study reservoirs among depths and seasonal  
287 periods (Figs 2-4, Figs S1-9). The concentration of dissolved CH<sub>4</sub> ranged up to four orders of magnitude from 0.06 to 213.64  
288 μM during the summer stratification (n = 96), and it was less variable during the winter mixing (n = 84) ranging only from  
289 0.02 to 0.69 μM. All depths were consistently supersaturated in CH<sub>4</sub> both during the stratification and mixing period (Table  
290 S1). The dissolved CH<sub>4</sub> concentration and the % of saturation values were significantly higher during the stratification period  
291 than during the mixing period (V = 78, p-value < 0.001; V = 78, p-value < 0.001, respectively). These differences in the  
292 concentration of dissolved CH<sub>4</sub> are coherent with the differences found in the CH<sub>4</sub> emissions from these reservoirs in the  
293 stratification and mixing periods (León-Palmero et al., 2020). The wide range in CH<sub>4</sub> concentrations found in this study  
294 covers from values reported in temperate lakes (Donis et al., 2017; Grossart et al., 2011; Tang et al., 2014; West et al., 2016),  
295 to those found in tropical lakes and reservoirs (Murase et al., 2003; Naqvi et al., 2018; Okuku et al., 2019; Roland et al.,  
296 2017). In the surface mixing layer during the stratification period (i.e., epilimnion), we found values from 0.06 to 8.18 μM  
297 (Table S1), which is about eighty times the maximum values found in the surface waters of Lake Kivu (Africa) by Roland et  
298 al., (2017) and similar to the concentrations reported in subtropical and tropical reservoirs (Musenze et al. 2014, and  
299 references therein).

300 The dissolved CH<sub>4</sub> profiles showed considerable differences among depths during the summer stratification (Figs.  
301 2a-4a, Figs S1a-9a, but were very homogeneous during the winter mixing in all the reservoirs (Figs. 2b-4b, Figs S1b-9b)  
302 (Table S1). Based on the differences found during the stratification period in the dissolved CH<sub>4</sub> profiles, we sorted the  
303 reservoirs in three types. The first type of CH<sub>4</sub> profile included six reservoirs that were characterized by an increase of the  
304 dissolved CH<sub>4</sub> from the oxycline to the anoxic bottom, just above the sediments, where CH<sub>4</sub> concentration reached its  
305 maximum. In these reservoirs, the oxycline may be spatially coupled to the thermocline, or not. When the oxycline and the  
306 thermocline were spatially coupled, the dissolved CH<sub>4</sub> concentration increased exponentially from the thermocline along the  
307 anoxic hypolimnion to the sediments. The reservoirs Béznar, San Clemente, and Iznájar showed this type of profile (Fig. 2a  
308 and Figs. S1a and S2a). The existence of a sizeable almost anoxic hypolimnion led to a massive accumulation of CH<sub>4</sub> in this  
309 layer. The differences in the CH<sub>4</sub> concentration between the surface and bottom waters were up to three orders of magnitude,  
310 as we found in Béznar (from the 0.25 to 56.17 μM; Fig. 2a), San Clemente (from the 0.23 to 45.15 μM; Fig S1a), and Iznájar  
311 (from the 0.82 μM to 213.64 μM; Fig. S2a). When the oxycline and the thermocline were not spatially coupled, the dissolved  
312 CH<sub>4</sub> concentration increased just above the sediments where the anoxic-oxic interface was near to the bottom. The reservoirs

313 Cubillas, La Bolera, and Francisco Abellán showed this profile type (Figs. S3a, S4a, and S5a). This accumulation of CH<sub>4</sub> in  
314 the hypolimnion and above sediments might be related to the high rates of methanogenesis in the sediments and its  
315 subsequent diffusion to the water column. Dissolved CH<sub>4</sub> concentration declines at the oxycline level, where the highest  
316 rates of CH<sub>4</sub> oxidation usually occur (Oswald et al., 2015, 2016). The CH<sub>4</sub> profiles in this group were similar to the ones  
317 found in tropical eutrophic and temperate reservoirs (Naqvi et al., 2018; West et al., 2016). The second profile type presents  
318 a small peak of metalimnetic CH<sub>4</sub>, concomitant with peaks of dissolved oxygen, chlorophyll-a, photosynthetic  
319 picoeukaryotes, and cyanobacteria (Fig. 3a). In the Negratín reservoir, we found the maximum concentration of CH<sub>4</sub> in the  
320 oxic hypolimnion. Unlike several previous works in lakes (Blees et al., 2015; Grossart et al., 2011; Khatun et al., 2019;  
321 Murase et al., 2003), we did not find a metalimnetic CH<sub>4</sub> maximum. Khatun et al., (2019) described the existence of a  
322 metalimnetic CH<sub>4</sub> maximum in ten out of 14 lakes. The metalimnetic CH<sub>4</sub> maximum may represent a physically driven CH<sub>4</sub>  
323 accumulation due to solubility differences with the temperature at the thermocline, the epilimnetic CH<sub>4</sub> losses by emission,  
324 and the lateral inputs from the littoral zone (Donis et al., 2017; Encinas Fernández et al., 2016; Hofmann et al., 2010). The  
325 metalimnetic CH<sub>4</sub> maximum can also be determined by biological factors including the light inhibition of the methane  
326 oxidation (Murase and Sugimoto, 2005; Tang et al., 2014) or the distinctive methane production by phytoplankton due to  
327 availability of nutrients, light or precursors at this layer (Khatun et al., 2019). The third profile type included five reservoirs,  
328 in which the dissolved CH<sub>4</sub> profile presented a CH<sub>4</sub> accumulation more significant in the epilimnion than in the hypolimnion.  
329 The reservoirs Jándula, Bermejales, Rules, El Portillo, and Colomera showed this profile type (Fig. 4a, Figs. S6a–9a). These  
330 reservoirs had a mean CH<sub>4</sub> concentration in the water column significantly lower than the reservoirs from the first type.  
331 Similar profiles have been reported in temperate (Tang et al., 2014) and tropical lakes (Murase et al., 2003).

### 332 **3. 2. CH<sub>4</sub> sources in the water column**

333 We found two well-differentiated groups of CH<sub>4</sub> data sorted by the dissolved oxygen (D.O.) concentration (Fig. S10), like in  
334 previous studies (Tang et al., 2014). The first dataset included the samples with a D.O. lower than 7.5 µM (n = 18, hereafter  
335 anoxic samples). These samples belong to the hypolimnion of the study reservoirs during the stratification period. The  
336 second dataset included the samples with D.O. higher than 7.5 µM (n = 160, hereafter oxic samples). All the samples from  
337 the mixing period (n = 82) and most of the samples from the stratification period (n = 78) belong to this second dataset. We  
338 found significant differences (W = 2632, p-value < 0.001) between the concentration of CH<sub>4</sub> in the anoxic samples (median =  
339 15.79 µM, min = 0.35 µM, max = 213.64 µM) and in the oxic samples (median = 0.15 µM, min = 0.02 µM, max = 8.17  
340 µM). Since these two groups of samples are different, we determined their sources and drivers separately (Table S2).

#### 341 **3. 2. 1. CH<sub>4</sub> sources in anoxic waters**

342 Archaeal methanogens are obligate anaerobes that decompose the organic matter and produce CH<sub>4</sub> in anoxic environments,  
343 as freshwater sediments. We analyzed the presence of the methanogenic *Archaea* in the anoxic samples of the water column

344 by targeting the gene *mcrA*. From the 77 samples selected for genetic analysis, twelve of them were anoxic. We did not  
345 detect the amplification of the *mcrA* gene in the PCR or the qPCR analysis in these twelve samples. Therefore, we assumed  
346 that the methanogenic *Archaea* were not present, as free-living microorganisms, in the water column of the anoxic samples.  
347 However, they may still be present in micro-anoxic zones in the water column (i.e., in the guts of zooplankton or within  
348 exopolymeric particles). Methanogenesis is a microbial process particularly sensitive to temperature (Marotta et al., 2014;  
349 Sepulveda-Jauregui et al., 2018; Yvon-Durocher et al., 2014). However, we did not find a significant relationship between  
350 the water temperature and the dissolved CH<sub>4</sub> concentration in the anoxic samples (n=17, p-value = 0.66). The no detection of  
351 the *mcrA* gene in the hypolimnetic waters and the absence of a relationship between the dissolved CH<sub>4</sub> and water  
352 temperature suggest that CH<sub>4</sub> production is not happening in the water column of the study reservoirs. We think that most  
353 methanogenic archaea must be present in the sediments, where they produce CH<sub>4</sub> that diffuses up to the water column  
354 producing vast accumulations of CH<sub>4</sub> in the hypolimnion.

355 Methanogenesis in the sediments may be affected by organic matter quantity and quality (West et al., 2012).  
356 Organic matter quantity is measured as the dissolved organic carbon concentration, whereas the organic matter quality  
357 usually is related to their phytoplanktonic vs terrestrial origin. In the study reservoirs, the dissolved organic carbon  
358 concentration did not show a significant relationship with the dissolved CH<sub>4</sub> concentration (n=12, p-value = 0.10, Table S2).  
359 We examined the importance of the autochthonous organic matter produced by primary producers using the total cumulative  
360 chlorophyll-a (Chl-a, mg m<sup>-2</sup>). The cumulative Chl-a is considered as a surrogate for the vertical export of the phytoplankton  
361 biomass in the whole water column. We obtained that the CH<sub>4</sub> concentrations in anoxic samples was correlated to the  
362 cumulative Chl-a following a power function (CH<sub>4</sub> = 3.0 10<sup>-4</sup> Cumulative Chl-a<sup>2.28</sup>; n=17, adj R<sup>2</sup>=0.40, p-value <0.01, Table  
363 S2) (Fig. 5). The autochthonous organic matter appeared to be a better predictor for the concentration of CH<sub>4</sub> in anoxic  
364 waters than the dissolved organic matter concentration. In the study reservoirs, the dissolved organic carbon concentration  
365 was significantly related to the age of the reservoirs and the forestry coverage in their watersheds (León-Palmero et al.,  
366 2019). Therefore, in terms of quality, the total pool of dissolved organic carbon may be more representative of the  
367 allochthonous, recalcitrant and more resistant to microbial degradation carbon fraction. In contrast, the autochthonous  
368 organic matter may represent a more labile and biodegradable fraction. Previous experimental studies have demonstrated that  
369 the addition of algal biomass on sediment cores increase the CH<sub>4</sub> production more than the addition of terrestrial organic  
370 matter (Schwarz et al., 2008; West et al., 2012, 2015). The stimulation of the methanogenesis rates appears to be related to  
371 the lipid content in phytoplankton biomass (West et al. 2015). West et al. (2016) found a significant relationship between the  
372 chlorophyll-a concentration in the epilimnion and the potential methanogenesis rates from sediment incubations. In this  
373 study, we corroborate the importance of the autochthonous-derived organic matter determining the CH<sub>4</sub> concentrations in  
374 anoxic waters. Since we did not detect the existence of the *mcrA* gene in the water column, we considered that the  
375 production of methane by methanogenic *Archaea* occurred primarily in the sediments and was affected by the sedimentation  
376 of organic matter derived from phytoplankton.

### 377 3. 2. 2. CH<sub>4</sub> sources in oxic waters

378 In this study, the concentration of dissolved CH<sub>4</sub> ranged from 0.02 μM to 8.18 μM, and all the samples of the oxic waters  
379 were supersaturated with values always above 800% and ranging more than two orders of magnitude (Table S1). To  
380 determine the origin of this CH<sub>4</sub> supersaturation we examined the following potential sources: (1) the vertical and lateral CH<sub>4</sub>  
381 transport from deep layers and littoral zones, (2) the in situ CH<sub>4</sub> production by methanogenic *Archaea* potentially tolerant to  
382 oxygen or by the methyl-phosphonate degradation under severe P-limitation, and 3) the in situ CH<sub>4</sub> production by processes  
383 associated to the phytoplanktonic community.

#### 384 Vertical and lateral CH<sub>4</sub>-transport from anoxic sediments to oxic waters

385 Several previous works have pointed out that CH<sub>4</sub> supersaturation in oxic waters can be explained by the vertical transport  
386 from the bottom sediments, and the lateral inputs from the littoral zones that are in contact with shallow sediments where  
387 methanogenesis occurs (Bastviken et al., 2004; Encinas Fernández et al., 2016; Michmerhuizen et al., 1996). To test the  
388 importance of the lateral and vertical transport explaining the concentration of CH<sub>4</sub> in the oxic waters of the study reservoirs,  
389 we used two morphometric parameters: the mean depth (m) as a proxy for the vertical transport and the shallowness index as  
390 a proxy for the lateral transport. The dissolved CH<sub>4</sub> concentration was an exponential decay function of the reservoir mean  
391 depth (Fig. 6a) both during the stratification period ( $\text{CH}_4 = 4.0 \cdot 10^{-2} e^{(50.0/\text{mean depth})}$ , adj R<sup>2</sup> = 0.95) and during the mixing  
392 period ( $\text{CH}_4 = 3.7 \cdot 10^{-2} e^{(22.9/\text{mean depth})}$ , adj R<sup>2</sup> = 0.54) (Fig. 6a). We observed that in reservoirs with a mean depth shallower  
393 than 16 meters, the dissolved CH<sub>4</sub> concentration increased exponentially (Fig. 6a). Several studies have proposed that the  
394 vertical transport of CH<sub>4</sub> from bottom sediments explains the supersaturation in surface waters (Rudd & Hamilton 1978,  
395 Michmerhuizen et al. 1996, Murase et al. 2003, Bastviken et al. 2004). However, the vertical diffusion rates of dissolved  
396 gases across the thermocline are too low in deep and thermally stratified systems and no movements of methane upwards  
397 from the hypolimnion have been detected (Rudd and Hamilton, 1978). However, in shallow reservoirs, the hydrostatic  
398 pressure might be reduced promoting CH<sub>4</sub> diffusion from the anoxic layers.

399 The shallowness index increases in elongated and dendritic reservoirs with more impact of the littoral zone and  
400 decreases in near-circular reservoirs, with low shoreline length per surface. However, we did not find a significant  
401 relationship between the shallowness index and the dissolved CH<sub>4</sub> concentration (Fig. 6b). One explanation for the absence  
402 of this relationship could be the relatively large size of the reservoirs. Although the reservoir size covered more than one  
403 order of magnitude (Table 1), all reservoirs have a size larger than 1 Km<sup>2</sup>. Previous studies have shown that CH<sub>4</sub> lateral  
404 diffusion may be an important process in areas near to the littoral zone and small lakes. Hofmann et al., (2010) found higher  
405 concentrations in the shallow littoral zones than in the open waters. DelSontro et al., (2018) predicted that lateral inputs from  
406 littoral zones to pelagic waters are more critical in small and round lakes than in large and elongated lakes. Nevertheless, the  
407 differences between the observations and predictions from the model suggested that these lateral inputs may not be enough

408 to explain CH<sub>4</sub> concentration in open waters, where in situ production may prevail over lateral transport (DelSontro et al.,  
409 2018).

#### 410 **In situ CH<sub>4</sub>-production by methanogenic *Archaea* or methyl-phosphonate degradation**

411 The ubiquitous CH<sub>4</sub> supersaturation found in oxic waters appear not to be fully explained by the vertical and lateral transport  
412 underlining that there is an in situ production of CH<sub>4</sub> as proposed by Bogard et al., (2014), DelSontro et al., (2018), and  
413 Grossart et al., (2011). We studied the presence of the methanogenic *Archaea* in the oxic samples by targeting the gene  
414 *mcrA*, but we were unable to detect this gene (Fig. S11). This result indicates that methanogenic *Archaea* were not present, at  
415 least as free-living microorganisms, in a significant number in the water column of the oxic samples. The classical  
416 methanogens (i.e., *Archaea* with the *mcrA* gene) are obligate anaerobes without the capacity to survive and produce CH<sub>4</sub>  
417 under aerobic conditions (Chistoserdova et al., 1998). Previous studies by Angel et al., (2011) and Angle et al., (2017)  
418 showed that methanogens might tolerate oxygen exposure in soils and Grossart et al., (2011) detected potential  
419 methanogenic *Archaea* attached to photoautotrophs in lake oxic waters. Unfortunately, we did not test their occurrence in  
420 large particles, phytoplankton or zooplankton guts, although some authors have detected them in these microsites particles  
421 (Angelis and Lee, 1994; Karl and Tilbrook, 1994).

422 We also considered the possibility of methylphosphonates degradation as an in situ CH<sub>4</sub> source. This metabolic  
423 pathway appears in the bacterioplankton under chronic starvation for phosphorus (Karl et al., 2008). Several pieces of  
424 evidence have shown that marine bacterioplankton can degrade the MPn and produce CH<sub>4</sub> through the C–P lyase activity in  
425 typically phosphorus starved environments, as the ocean gyres (Beverdors et al., 2010; Carini et al., 2014; Repeta et al.,  
426 2016; Teikari et al., 2018; del Valle and Karl, 2014). Freshwater bacteria can also degrade the MPn and produce CH<sub>4</sub>, as it  
427 has been demonstrated in Lake Matano (Yao et al., 2016b, 2016a). Lake Matano is an ultra-oligotrophic lake with a severe P  
428 deficiency (below 0.050 μmol P L<sup>-1</sup>) due to the permanent stratification, iron content, and extremely low nutrient inputs  
429 (Crowe et al., 2008; Sabo et al., 2008). The ratio of dissolved inorganic nitrogen (DIN) to total phosphorus (TP) (μmol N:  
430 μmol P) is widely used to evaluate P-limitation (Morris and Lewis, 1988). DIN:TP ratios greater than 4 are indicative of  
431 phosphorus limitation (Axler et al., 1994). In the study reservoirs, the TP concentration ranged from 0.13 to 1.85 μmol P L<sup>-1</sup>  
432 during the stratification period, and from 0.10 to 2.17 μmol P L<sup>-1</sup> during the mixing period. The DIN:TP ratio ranged from  
433 15 to 985 during the stratification period, and from 28 to 690 during the mixing period. The more severe the P-limitation  
434 conditions, the higher the CH<sub>4</sub> production by methylphosphonates degradation is. However, we did not find a significant  
435 relationship between the DIN:TP ratio and the CH<sub>4</sub> concentration (Fig. 7). We also analyzed the presence and abundance of  
436 the gene *phnJ*, which encodes the enzyme complex C–P lyase that hydrolyzes the MPn and changes in response to phosphate  
437 availability. We did not detect the *phnJ* gene in the PCR or the qPCR analysis in any of the study samples (Fig. S12). These  
438 results indicate that the MPn degradation was not a quantitatively relevant source of CH<sub>4</sub> in the oxic waters of the study  
439 reservoirs. Our results are in concordance with Grossart et al. (2011), who did not detect CH<sub>4</sub> production by adding inorganic

440 phosphate or methylphosphonates to lake samples in laboratory experiments. Although we used different methodologies,  
441 both studies may indicate that MPn degradation is only an important source of CH<sub>4</sub> in ultra-oligotrophic systems, as Lake  
442 Matano or ocean gyres.

#### 443 **In situ CH<sub>4</sub>-production coupled to photosynthetic organisms**

444 In the study reservoirs, we analyzed the relationship between photosynthetic organisms and the dissolved CH<sub>4</sub> concentration  
445 using the gross primary production (GPP, g O<sub>2</sub> m<sup>-3</sup> d<sup>-1</sup>), net ecosystem production (NEP, g O<sub>2</sub> m<sup>-3</sup> d<sup>-1</sup>), the concentration of  
446 chlorophyll-a (Chl-a, µg L<sup>-1</sup>), and the abundance of photosynthetic picoeukaryotes (PPEs, cell mL<sup>-1</sup>) and cyanobacteria  
447 (CYA, cell mL<sup>-1</sup>). We determined GPP and NEP just once per reservoir during the stratification period (i.e., n=12).

448 The PPEs are essential components of the marine and freshwater phytoplankton, and they are eukaryotes with a size  
449 of 3.0 µm or less. In the freshwaters, the PPEs include species from different phyla, as unicellular *Chlorophyta* (green algae),  
450 and *Haptophyta*. Using optical microscopy, we determined the main groups of photosynthetic picoeukaryotes in the study  
451 reservoirs. PPEs were non-colonial green algae from the order *Chlorococcales* (class *Chlorophyceae*, phylum *Chlorophyta*),  
452 and the genus *Chrysochromulina* spp., (class *Coccolithophyceae*, phylum *Haptophyta*). The cyanobacteria detected were  
453 mainly phycoerythrin-rich picocyanobacteria, although we also detected phycocyanin-rich picocyanobacteria in one  
454 reservoir (Béznar). We show the vertical profiles of the Chl-a concentration and the abundance of PPEs and CYA profiles of  
455 each reservoir in Figs. 2-4 and Figs. S1-S9. We also report the minimum, the quartiles, and the maximum values for the Chl-  
456 a concentration and the abundance of PPEs and CYA during the stratification and the mixing periods in Table S2. The  
457 abundance of cyanobacteria ranged from 1.51 x 10<sup>3</sup> to 2.04 x 10<sup>5</sup> cells mL<sup>-1</sup> and was more than one order of magnitude higher  
458 than the abundance of PPEs that ranged from 32 to 7.45 x 10<sup>3</sup> cells mL<sup>-1</sup>.

459 We found that the relationship between the gross primary production and the dissolved CH<sub>4</sub> concentration was only  
460 marginally significant (p-value = 0.077, n = 12) and not significant with the net ecosystem production (Table 3). The Chl-a  
461 concentration showed a significant relationship with the GPP (p-value < 0.01, n = 12, adj R<sup>2</sup> = 0.55), but the abundance of  
462 cyanobacteria or the abundance of the photosynthetic picoeukaryotes did not show a significant relationship with the GPP  
463 (p-value = 0.911, n = 12; p-value = 0.203, n = 12, respectively). We found significant power relationships between the Chl-a  
464 concentration, the abundance of photosynthetic picoeukaryotes, and the abundance of cyanobacteria with the concentration  
465 of dissolved CH<sub>4</sub> during the stratification period (Fig. 8a, 8b, and 8c respectively, and Table 3). During the mixing period,  
466 the only significant predictor of the dissolved CH<sub>4</sub> concentration was the abundance of photosynthetic picoeukaryotes (Fig.  
467 8b). The variance explained, and the slope of the relationship (i.e. the exponent in the power relationship) between the  
468 dissolved CH<sub>4</sub> and the abundance of photosynthetic picoeukaryotes was higher during the stratification than during the  
469 mixing (Table 3). By comparing the stratification slopes, the effect per cell of PPEs on CH<sub>4</sub> concentration was slightly  
470 higher than the impact of cyanobacteria (Table 3). These results agree with previous studies that showed a closed link  
471 between the CH<sub>4</sub> concentration and the photosynthetic organisms, primary production, or chlorophyll-a concentration  
472 (Bogard et al., 2014; Grossart et al., 2011; Schmidt and Conrad, 1993; Tang et al., 2014). In this study, we show that the

473 PPEs abundance was a better predictor of the CH<sub>4</sub> concentration than the abundance of cyanobacteria. In the study  
474 reservoirs, the PPEs group included members from green algae and *Haptophyta*, which are regular components of the marine  
475 plankton. Therefore, these results may be relevant also for marine waters. Cyanobacteria have received more attention as  
476 potential producers of CH<sub>4</sub> in oxic conditions than photosynthetic picoeukaryotes (Berg et al., 2014; Bižić et al., 2020;  
477 Teikari et al., 2018). Klintzsch et al., (2019) demonstrated that widespread marine and freshwater haptophytes as *Emiliana*  
478 *huxleyi*, *Phaeocystis globosa* and *Chrysochromulina sp.* produce CH<sub>4</sub> under oxic conditions. They also observed that the cell  
479 abundances were significantly related to the amount of CH<sub>4</sub> produced. Interestingly, *Chrysochromulina* was one of the  
480 genera of PPEs that we detected in the study reservoirs. Grossart et al. (2011) also found CH<sub>4</sub> production in laboratory  
481 cultures of cyanobacteria and green algae.

482 Overall, these results indicate a clear association between the CH<sub>4</sub> production and the photosynthetic organisms  
483 from both *Eukarya* (picoeukaryotes) and *Bacteria* (cyanobacteria) domains. The pathways involved in the CH<sub>4</sub> production  
484 may be related to the central photosynthetic metabolism or the release of methylated by-products different from  
485 methylphosphonates during the photosynthesis. Previous studies demonstrated the CH<sub>4</sub> production in laboratory cultures  
486 using <sup>13</sup>C-labeled bicarbonate in haptophytes (Klintzsch et al., 2019; Lenhart et al., 2016), in marine, freshwater, and  
487 terrestrial cyanobacteria (Bižić et al., 2020), and major groups of phytoplankton (Hartmann et al., 2020). In these studies, the  
488 photosynthetic organisms uptake bicarbonate in the reductive pentose phosphate cycle (Calvin-Benson cycle) (Berg, 2011;  
489 Burns and Beardall, 1987). Therefore, CH<sub>4</sub> production may be a common pathway in the central metabolism of  
490 photosynthesis of all the cyanobacteria and algae in freshwaters and marine environments.

491 On the other hand, the production of CH<sub>4</sub> can also be related to the production of methylated compounds during  
492 photosynthesis. Lenhart et al. (2016) and Klintzsch et al., (2019) also detected the CH<sub>4</sub> production in cultures from the  
493 sulfur-bound methyl group of the methionine and methyl thioethers. Common substances as methionine can act as a methyl-  
494 group donor during the CH<sub>4</sub> production in plants and fungi (Lenhart et al. 2012, 2015). Besides, algae use part of the  
495 methionine for the synthesis of dimethylsulfoniopropionate (DMSP), an abundant osmolyte, the precursor of dimethyl  
496 sulfide (DMS), and dimethylsulphoxide (DMSO). These methylated substances produce methane during their degradation  
497 (Damm et al., 2008, 2010, 2015; Zindler et al., 2013). Bižić-Ionescu et al., (2018) also suggested that CH<sub>4</sub> could be produced  
498 from methylated amines under oxic conditions. These substances, together with other organosulphur compounds, can also  
499 produce CH<sub>4</sub> abiotically (Althoff et al., 2014; Bižić-Ionescu et al., 2018). The production of DMSP, DMS, and other  
500 methylated substances as isoprene, has been extensively studied in marine phytoplankton, showing that taxa as  
501 photosynthetic picoeukaryotes and the cyanobacteria are relevant sources (Shaw et al., 2003; Yoch, 2002). Recent studies  
502 have also reported that freshwater algae and cyanobacteria also produced DMS and isoprene (Steinke et al., 2018). Further  
503 studies are needed to quantify the potential role of all these methylated by-products as potential CH<sub>4</sub> sources quantitatively  
504 relevant in freshwaters.



### 505 3. 2. 3. Modeling the CH<sub>4</sub> production in oxic waters

506 The explanation of the CH<sub>4</sub> supersaturation in oxic waters in relatively large systems rely on the interaction of several  
507 processes as the transport from anoxic environments and the biological activity (DelSontro et al., 2018). In this study, we  
508 found that vertical transport (mean depth as surrogate), water temperature, and the abundance of photosynthetic  
509 picoeukaryotes and cyanobacteria had a significant effect on the dissolved CH<sub>4</sub> concentration. We combined these  
510 explanatory variables with significant effects using generalized additive models (GAMs). The GAM model for the  
511 stratification period (n=78) had a fit deviance of 82.7% and an explained variance (adj R<sup>2</sup>) of 81.4 % (Table S3). The  
512 explanatory variables, in decreasing order, were: the photosynthetic picoeukaryotes abundance (log<sub>10</sub> PPEs), the reservoir  
513 mean depth, the cyanobacteria abundance (log<sub>10</sub> CYA), and the water temperature (Fig. 9a). The function obtained was:  
514  $\text{Log}_{10} \text{CH}_4 = -4.05 + 3.4 \cdot 10^{-1} \text{Log}_{10} \text{PPEs} + e^{(6.7/\text{mean depth})} + 1.7 \cdot 10^{-1} \text{Log}_{10} \text{CYA} + 2.7 \cdot 10^{-2} \text{Temperature}$ . The abundance of  
515 PPEs was the variable explaining most of the variance of dissolved CH<sub>4</sub> concentration (Log<sub>10</sub> CH<sub>4</sub>) during the stratification  
516 period, with an effect higher than the cyanobacteria abundance. The panels b to e in Fig. 9 show the partial responses of each  
517 explanatory variable.

518 The GAM model for the mixing period (n=82) only included two explanatory variables: the reservoir mean depth  
519 and the abundance of the photosynthetic picoeukaryotes. The reservoir mean depth was the variable explaining most of the  
520 variance of the dissolved CH<sub>4</sub> concentration (Log<sub>10</sub> CH<sub>4</sub>) during the mixing period, closely followed by the abundance of  
521 PPEs (Fig. 10a). We observed that the function of the effect of the mean depth on the CH<sub>4</sub> concentration changed between  
522 the two periods (Fig. 9c and Fig 10b). The function was more linear during the mixing period than during the stratification  
523 period likely because the mixed water column enabled the more uniform distribution of the CH<sub>4</sub> produced in the sediment,  
524 while the thermocline acted as a barrier to the diffusion during the stratification period. The model function for the mixing  
525 period was:  $\text{Log}_{10} \text{CH}_4 = -2.07 + 1.5 e^{(-0.04 \text{ mean depth})} + 1.8 \cdot 10^{-1} \text{Log}_{10} \text{PPEs}$ , with a fit deviance of 53.9 % and an explained  
526 variance (adj R<sup>2</sup>) of 52.1 % (Table S3). In Figure 10b and 10c, we show the partial response plots for these two variables.  
527 The results show that the abundance of photosynthetic picoeukaryotes can be key for explaining the dissolved CH<sub>4</sub>  
528 concentration in oxic waters, even though they have received less attention than cyanobacteria in previous studies (Berg et  
529 al., 2014; Bižić et al., 2020; Teikari et al., 2018). Finally, we have also included a simple model to explain the dissolved CH<sub>4</sub>  
530 concentration (Log<sub>10</sub> CH<sub>4</sub>) using the data of both periods (n=160) and including widely used variables like the water  
531 temperature (°C), mean depth (m), and chlorophyll-a concentration (Chl-a, µg L<sup>-1</sup>) for future comparisons. The function of  
532 this model is:  $\text{Log}_{10} \text{CH}_4(\mu\text{M}) = -2.02 + 0.05 \text{Temperature} + e^{(7.73/\text{mean depth})} - e^{(-0.05 \text{Log}_{10}(\text{Chl-a}))}$ . This GAM model had a fit  
533 deviance of 69.3 % and an explained variance (adj R<sup>2</sup>) of 68 % (Table S3).

534 Overall, during the stratification period, the in situ CH<sub>4</sub> production was coupled to the abundance of photosynthetic  
535 picoeukaryotes in oxic waters (Fig. 9a) and mean depths. This CH<sub>4</sub> source due to photosynthetic picoeukaryotes can be  
536 crucial in large, deep lakes and reservoirs, and the open ocean since the impact of the CH<sub>4</sub> transport from sediments (i.e.,  
537 mean depth) decreases with increasing depths. In deeper reservoirs, the thermal stratification during the summer produced

538 that the vertical diffusion rates of CH<sub>4</sub> from sediments is limited. Rudd and Hamilton, (1978) did not detect any movement  
539 of CH<sub>4</sub> upwards from the hypolimnion during the stratification. Previous studies have suggested that the CH<sub>4</sub> produced in the  
540 oxic water column is the primary source of CH<sub>4</sub> in large and deep lakes (Bogard et al., 2014; DelSontro et al., 2018; Donis et  
541 al., 2017; Günthel et al., 2019). Günthel et al., (2019) shown that large lakes have a lower sediment area in comparison to the  
542 volume of the surface mixed layer than small lakes and that this fact determines the higher contribution of the oxic methane  
543 production to surface emission in large (>1 Km<sup>2</sup>) lakes than in small ones. The photosynthetic picoeukaryotes identified in  
544 the study reservoirs are considered indicators of eutrophic conditions and they are bloom-forming genera  
545 (i.e., *Chlorococcales* and *Chrysochromulina* spp.) (Edwardsen and Paasche, 1998; Reynolds, 1984; Willén, 1987). Global  
546 future estimations suggest a rise in eutrophication and algal bloom over the next century due to climate change and the  
547 growing human population (Beaulieu et al., 2019). In that situation, photosynthetic picoeukaryotes  
548 as *Chlorococcales* and *Chrysochromulina* spp., and cyanobacteria, would lead to an increment in CH<sub>4</sub> production and  
549 emissions. Further studies are needed to understand better the role of the photosynthetic picoeukaryotes in the production of  
550 CH<sub>4</sub> in oxic waters, and to quantify their influence in the methane supersaturation and CH<sub>4</sub> fluxes from inland and oceanic  
551 waters.

#### 552 **4 Conclusions**

553 The dissolved CH<sub>4</sub> concentration in the study reservoirs showed a considerable variability (i.e. up to four orders of  
554 magnitude) and presented a clear seasonality. Surface waters were always supersaturated in CH<sub>4</sub>. The concentration of CH<sub>4</sub>  
555 was closely linked to the photosynthetic organisms. In the anoxic waters, the depth-cumulative chlorophyll-a concentration,  
556 a proxy for the phytoplanktonic biomass exported to sediments, determined the CH<sub>4</sub> concentration. In the oxic waters, we  
557 considered different potential CH<sub>4</sub> sources, including the vertical and lateral transport of CH<sub>4</sub> from anoxic zones and *in situ*  
558 production. The mean depth of the reservoirs, as a surrogate of the CH<sub>4</sub> transport from sediment to the oxic waters,  
559 contributed in shallow systems. We did not detect methanogenic *Archaea* or methylphosphonates degradation target genes  
560 (i.e. *mcrA* and *phnJ* genes, respectively), which suggests that these pathways are not responsible for the in situ production of  
561 CH<sub>4</sub> in the oxic waters of the study reservoirs. We found that dissolved CH<sub>4</sub> was coupled to the abundance of photosynthetic  
562 picoeukaryotes (PPEs) during both periods and to chlorophyll-a concentration and the abundance of and cyanobacteria  
563 during the stratification period. These PPEs were non-colonial green algae from the order *Chlorococcales*  
564 (class *Chlorophyceae*, phylum *Chlorophyta*), and the genus *Chrysochromulina* spp., (class *Coccolithophyceae*, phylum  
565 *Haptophyta*). Finally, we combined all the explanatory variables with significant effects and determined their relative  
566 contribution to the CH<sub>4</sub> concentration using generalized additive models (GAMs). The abundance of PPEs was the variable  
567 explaining most of the variance of dissolved CH<sub>4</sub> concentration during the stratification period, with an effect higher than the  
568 cyanobacteria abundance. During the mixing period, the reservoir mean depth and the abundance of the PPEs were the only  
569 drivers for CH<sub>4</sub> concentration. Our findings show that the abundance of PPEs can be relevant for explaining the dissolved

570 CH<sub>4</sub> concentration in oxic waters of large lakes and reservoirs.

571 **Data availability**

572 Additional figures and tables can be found in the supplementary information. The dataset associated with this manuscript  
573 will be available at Pangaea: Dissolved concentrations of CH<sub>4</sub>, nutrients, and biological parameters in the water column of  
574 twelve Mediterranean reservoirs in Southern Spain (<https://doi.org/10.1594/PANGAEA.912535>) and Primary production of  
575 twelve Mediterranean reservoirs in Southern Spain (<https://doi.org/10.1594/PANGAEA.912555>).

576 **Author contribution**

577 E.L.-P., R.M.-B. and I.R. contributed equally to this work. R.M.-B. and I.R. designed the study and obtained the funds. E.L.-  
578 P., R.M.-B., and I.R. contributed to data acquisition during the reservoir samplings. E.L.-P. processed most of the chemical  
579 and biological samples. A.C. performed the flow cytometry and part of the molecular analysis, and A.S. collaborated with  
580 the dissolved CH<sub>4</sub> analysis using gas chromatography. E.L.-P., R.M.-B. and I.R. analyzed the data and discussed the results.  
581 E.L.-P. wrote the first draft manuscript, which was complemented by significant contributions of R.M.-B. and I.R.

582 **Competing interests**

583 The authors declare that the research was conducted in the absence of any commercial or financial relationships that could be  
584 construed as a potential conflict of interest.

585 **Acknowledgements**

586 This research was funded by the project HERA (CGL2014-52362-R) to IR and RM-B of the Spanish Ministry of Economy  
587 and Competitiveness, the Modelling Nature Scientific Unit (UCE.PP2017.03) and the Consejería de Economía,  
588 Conocimiento, Empresas y Universidad from Andalucía and European Regional Development Fund (ERDF), ref.  
589 SOMM17/6109/UGR to IR. E.L.-P and A. S. were supported by PhD fellowships from the Ministry of Education, Culture  
590 and Sports (FPU014/02917 and FPU2014-04048, respectively). A. C.-R. was supported by the Youth Employment Initiative  
591 (YEI) from the Junta de Andalucía and financed by the European Commission (Ref 6017). We specially thank to Eulogio  
592 Corral for helping in the field, Dr. Jesús Forja, and Dra. Teodora Ortega for helping with gas chromatography analysis at the  
593 University of Cádiz, and Dr. David Fernández Moreno from the Department of Botany at the University of Granada for the  
594 taxonomical identification of the phytoplankton community. We thank the Hydrological Confederations of Guadalquivir and  
595 Sur to facility the reservoirs sampling.

596

597 **References**

- 598 Althoff, F., Benzing, K., Comba, P., McRoberts, C., Boyd, D. R., Greiner, S. and Keppler, F.: Abiotic methanogenesis from  
599 organosulphur compounds under ambient conditions, *Nat. Commun.*, 5, 4205, doi:10.1038/ncomms5205, 2014.
- 600 Álvarez-Salgado, X. A. and Miller, A. E. J.: Simultaneous determination of dissolved organic carbon and total dissolved  
601 nitrogen in seawater by high temperature catalytic oxidation: conditions for precise shipboard measurements, *Mar.*  
602 *Chem.*, 62(3), 325–333, doi:10.1016/S0304-4203(98)00037-1, 1998.
- 603 Angel, R., Matthies, D. and Conrad, R.: Activation of Methanogenesis in Arid Biological Soil Crusts Despite the Presence of  
604 Oxygen, *PLOS ONE*, 6(5), e20453, doi:10.1371/journal.pone.0020453, 2011.
- 605 Angelis, M. A. de and Lee, C.: Methane production during zooplankton grazing on marine phytoplankton, *Limnol.*  
606 *Oceanogr.*, 39(6), 1298–1308, doi:10.4319/lo.1994.39.6.1298, 1994.
- 607 Angle, J. C., Morin, T. H., Solden, L. M., Narrowe, A. B., Smith, G. J., Borton, M. A., Rey-Sanchez, C., Daly, R. A.,  
608 Mirfenderesgi, G., Hoyt, D. W., Riley, W. J., Miller, C. S., Bohrer, G. and Wrighton, K. C.: Methanogenesis in  
609 oxygenated soils is a substantial fraction of wetland methane emissions, *Nat. Commun.*, 8, doi:10.1038/s41467-017-  
610 01753-4, 2017.
- 611 Aronow, S.: Shoreline development ratio, in *Beaches and Coastal Geology*, pp. 754–755, Springer US, Boston, MA., 1982.
- 612 Axler, R. P., Rose, C. and Tikkanen, C. A.: Phytoplankton Nutrient Deficiency as Related to Atmospheric Nitrogen  
613 Deposition in Northern Minnesota Acid-Sensitive Lakes, *Can. J. Fish. Aquat. Sci.*, 51(6), 1281–1296,  
614 doi:10.1139/f94-128, 1994.
- 615 Baird, R. B., Eaton, A. D., Clesceri, L. S. and others: Standard methods for the examination of water and wastewater, edited  
616 by E. W. Rice, American Public Health Association Washington, DC., 2012.
- 617 Bastviken, D., Cole, J., Pace, M. and Tranvik, L.: Methane emissions from lakes: Dependence of lake characteristics, two  
618 regional assessments, and a global estimate, *Glob. Biogeochem. Cycles*, 18(4), 1–12, doi:10.1029/2004GB002238,  
619 2004.
- 620 Bastviken, D., Tranvik, L. J., Downing, J. A., Crill, P. M. and Enrich-Prast, A.: Freshwater Methane Emissions Offset the  
621 Continental Carbon Sink, *Science*, 331(6013), 1–12, doi:10.1126/science.1196808, 2011.
- 622 Beaulieu, J. J., DelSontro, T. and Downing, J. A.: Eutrophication will increase methane emissions from lakes and  
623 impoundments during the 21st century, *Nat. Commun.*, 10(1), 1375, doi:10.1038/s41467-019-09100-5, 2019.
- 624 Berg, A., Lindblad, P. and Svensson, B. H.: Cyanobacteria as a source of hydrogen for methane formation, *World J.*  
625 *Microbiol. Biotechnol.*, 30(2), 539–545, doi:10.1007/s11274-013-1463-5, 2014.
- 626 Berg, I. A.: Ecological Aspects of the Distribution of Different Autotrophic CO<sub>2</sub> Fixation Pathways, *Appl. Environ.*  
627 *Microbiol.*, 77(6), 1925–1936, doi:10.1128/AEM.02473-10, 2011.
- 628 Beversdorf, L. J., White, A. E., Björkman, K. M., Letelier, R. M. and Karl, D. M.: Phosphonate metabolism by  
629 *Trichodesmium* IMS101 and the production of greenhouse gases, *Limnol. Oceanogr.*, 55(4), 1768–1778,

630 doi:10.4319/lo.2010.55.4.1768, 2010.

631 Bižić, M., Klintzsch, T., Ionescu, D., Hindiyeh, M. Y., Günthel, M., Muro-Pastor, A. M., Eckert, W., Urich, T., Keppler, F.  
632 and Grossart, H.-P.: Aquatic and terrestrial cyanobacteria produce methane, *Science Advances*, 6(3), 9,  
633 doi:10.1126/sciadv.aax5343, 2020.

634 Bižić-Ionescu, M., Ionescu, D., Günthel, M., Tang, K. W., & Grossart, H. P. (2018). Oxidic methane cycling: New evidence  
635 for methane formation in Oxidic lake water. *Biogenesis of Hydrocarbons, edited by: Stams, AJ M and Souana, DZ,*  
636 *Springer International Publishing, Basel*, 1-22.

637 Brees, J., Niemann, H., Erne, M., Zopf, J., Schubert, C. J. and Lehmann, M. F.: Spatial variations in surface water methane  
638 super-saturation and emission in Lake Lugano, southern Switzerland, *Aquat. Sci.*, 77(4), 535–545,  
639 doi:10.1007/s00027-015-0401-z, 2015.

640 Bogard, M. J., del Giorgio, P. A., Boutet, L., Chaves, M. C. G., Prairie, Y. T., Merante, A. and Derry, A. M.: Oxidic water  
641 column methanogenesis as a major component of aquatic CH<sub>4</sub> fluxes, *Nat. Commun.*, 5, 5350,  
642 doi:10.1038/ncomms6350, 2014.

643 Boström, K. H., Simu, K., Hagström, Å. and Riemann, L.: Optimization of DNA extraction for quantitative marine  
644 bacterioplankton community analysis, *Limnol. Oceanogr. Methods*, 2(11), 365–373, doi:10.4319/lom.2004.2.365,  
645 2004.

646 Burns, B. D. and Beardall, J.: Utilization of inorganic carbon by marine microalgae, *J. Exp. Mar. Biol. Ecol.*, 107(1), 75–86,  
647 doi:10.1016/0022-0981(87)90125-0, 1987.

648 Carini, P., White, A. E., Campbell, E. O. and Giovannoni, S. J.: Methane production by phosphate-starved SAR11  
649 chemoheterotrophic marine bacteria, *Nat. Commun.*, 5, 4346, doi:10.1038/ncomms5346, 2014.

650 Cellamare, M., Rolland, A. and Jacquet, S.: Flow cytometry sorting of freshwater phytoplankton, *J. Appl. Phycol.*, 22(1),  
651 87–100, doi:10.1007/s10811-009-9439-4, 2010.

652 Chistoserdova, L., Vorholt, J. A., Thauer, R. K. and Lidstrom, M. E.: C1 Transfer Enzymes and Coenzymes Linking  
653 Methylophilic Bacteria and Methanogenic Archaea, *Science*, 281(5373), 99–102, doi:10.1126/science.281.5373.99,  
654 1998.

655 Cole, J. J., Pace, M. L., Carpenter, S. R. and Kitchell, J. F.: Persistence of net heterotrophy in lakes during nutrient addition  
656 and food web manipulations, *Limnol. Oceanogr.*, 45(8), 1718–1730, doi:10.4319/lo.2000.45.8.1718, 2000.

657 Collier, J. L.: Flow Cytometry and the Single Cell in Phycology, *J. Appl. Phycol.*, 36(4), 628–644, doi:10.1046/j.1529-  
658 8817.2000.99215.x, 2000.

659 Corzo, A., Jimenez-Gomez, F., Gordillo, F., Garcia-Ruiz, R. and Niell, F.: Synechococcus and Prochlorococcus-like  
660 populations detected by flow cytometry in a eutrophic reservoir in summer., *J. Plankton Res.*, 21(8), 1575–1581,  
661 doi:10.1093/plankt/21.8.1575, 1999.

662 Crowe, S. A., O'Neill, A. H., Katsev, S., Hehanussa, P., Haffner, G. D., Sundby, B., Mucci, A. and Fowle, D. A.: The  
663 biogeochemistry of tropical lakes: A case study from Lake Matano, Indonesia, *Limnol. Oceanogr.*, 53(1), 319–331,

664 doi:10.4319/lo.2008.53.1.0319, 2008.

665 Damm, E., Kiene, R. P., Schwarz, J., Falck, E. and Dieckmann, G.: Methane cycling in Arctic shelf water and its relationship  
666 with phytoplankton biomass and DMSP, *Mar. Chem.*, 109(1–2), 45–59, doi:10.1016/j.marchem.2007.12.003, 2008.

667 Damm, E., Helmke, E., Thoms, S., Schauer, U., Nöthig, E., Bakker, K. and Kiene, R. P.: Methane production in aerobic  
668 oligotrophic surface water in the central Arctic Ocean, *Biogeosciences*, 7(3), 1099–1108, doi:10.5194/bg-7-1099-  
669 2010, 2010.

670 Damm, E., Thoms, S., Beszczynska-Möller, A., Nöthig, E. M. and Kattner, G.: Methane excess production in oxygen-rich  
671 polar water and a model of cellular conditions for this paradox, *Polar Sci.*, 9(3), 327–334,  
672 doi:10.1016/j.polar.2015.05.001, 2015.

673 Deemer, B. R., Harrison, J. A., Li, S., Beaulieu, J. J., DelSontro, T., Barros, N., Bezerra-Neto, J. F., Powers, S. M., dos  
674 Santos, M. A. and Vonk, J. A.: Greenhouse Gas Emissions from Reservoir Water Surfaces: A New Global Synthesis,  
675 *BioScience*, 66(11), 949–964, doi:10.1093/biosci/biw117, 2016.

676 DelSontro, T., del Giorgio, P. A. and Prairie, Y. T.: No Longer a Paradox: The Interaction Between Physical Transport and  
677 Biological Processes Explains the Spatial Distribution of Surface Water Methane Within and Across Lakes,  
678 *Ecosystems*, 21(6), 1073–1087, doi:10.1007/s10021-017-0205-1, 2018.

679 Dlugokencky, E. J.: Trends in Atmospheric Methane. Globally averaged marine surface monthly mean data., NOAA/ESRL.  
680 [online] Available from: [www.esrl.noaa.gov/gmd/ccgg/trends\\_ch4/](http://www.esrl.noaa.gov/gmd/ccgg/trends_ch4/), 2019.

681 Donis, D., Flury, S., Stöckli, A., Spangenberg, J. E., Vachon, D. and McGinnis, D. F.: Full-scale evaluation of methane  
682 production under oxic conditions in a mesotrophic lake, *Nat. Commun.*, 8(1), 1661, doi:10.1038/s41467-017-01648-  
683 4, 2017.

684 Edvardsen, B. and Paasche, E.: Bloom dynamics and physiology of *Prymnesium* and *Chrysochromulina*, *NATO ASI*  
685 *SERIES G ECOLOGICAL SCIENCES*, 41, 193–208, 1998.

686 Encinas Fernández, J., Peeters, F. and Hofmann, H.: On the methane paradox: Transport from shallow water zones rather  
687 than in situ methanogenesis is the major source of CH<sub>4</sub> in the open surface water of lakes, *JGR: Biogeosciences*,  
688 121(10), 2717–2726, doi:10.1002/2016JG003586, 2016.

689 Fox, A., Kwapinski, W., Griffiths, B. S. and Schmalenberger, A.: The role of sulfur- and phosphorus-mobilizing bacteria in  
690 biochar-induced growth promotion of *Lolium perenne*, *FEMS Microbiol. Ecol.*, 90(1), 78–91, doi:10.1111/1574-  
691 6941.12374, 2014.

692 Fox, J. and Weisberg, S.: *An R Companion to Applied Regression*, Second., Sage, Thousand Oaks CA. [online] Available  
693 from: <http://socserv.socsci.mcmaster.ca/jfox/Books/Companion>, 2011.

694 Gasol, J. M. and Giorgio, P. A. del: Using flow cytometry for counting natural planktonic bacteria and understanding the  
695 structure of planktonic bacterial communities, *Sci. Mar.*, 64(2), 197–224, doi:10.3989/scimar.2000.64n2197, 2000.

696 Gomez-Garcia, M. R., Davison, M., Blain-Hartnung, M., Grossman, A. R. and Bhaya, D.: Alternative pathways for  
697 phosphonate metabolism in thermophilic cyanobacteria from microbial mats, *ISME J.*, 5(1), 141–149,

698 doi:10.1038/ismej.2010.96, 2011.

699 Grabarse, W., Mahlert, F., Duin, E. C., Goubeaud, M., Shima, S., Thauer, R. K., Lamzin, V. and Ermler, U.: On the  
700 mechanism of biological methane formation: structural evidence for conformational changes in methyl-coenzyme M  
701 reductase upon substrate binding, *J. Mol. Biol.*, 309(1), 315–330, doi:10.1006/jmbi.2001.4647, 2001.

702 Gross, J. and Ligges, U.: nortest: Tests for Normality. [online] Available from: <https://CRAN.R-project.org/package=nortest>  
703 (Accessed 3 June 2018), 2015.

704 Grossart, H.-P., Frindte, K., Dziallas, C., Eckert, W. and Tang, K. W.: Microbial methane production in oxygenated water  
705 column of an oligotrophic lake, *PNAS*, 108(49), 19657–19661, doi:10.1073/pnas.1110716108, 2011.

706 Günthel, M., Donis, D., Kirillin, G., Ionescu, D., Bizic, M., McGinnis, D. F., Grossart, H.-P. and Tang, K. W.: Contribution  
707 of oxic methane production to surface methane emission in lakes and its global importance, *Nat. Commun.*, 10(1), 1–  
708 10, doi:10.1038/s41467-019-13320-0, 2019.

709 Hartmann, J. F., Günthel, M., Klintzsch, T., Kirillin, G., Grossart, H.-P., Keppler, F. and Isenbeck-Schröter, M.: High  
710 Spatiotemporal Dynamics of Methane Production and Emission in Oxic Surface Water, *Environ. Sci. Technol.*, 54(3),  
711 1451–1463, doi:10.1021/acs.est.9b03182, 2020.

712 Hastie, T. and Tibshirani, R.: Generalized Additive Models, *Statist. Sci.*, 1(3), 297–310, doi:10.1214/ss/1177013604, 1986.

713 Hastie, T. and Tibshirani, R. J.: Generalized additive models, London: Chapman and Hall., 1990.

714 Hofmann, H., Federwisch, L. and Peeters, F.: Wave-induced release of methane: Littoral zones as source of methane in  
715 lakes, *Limnology and Oceanography*, 55(5), 1990–2000, doi:10.4319/lo.2010.55.5.1990, 2010.

716 Jähne, B., Münnich, K. O., Bössinger, R., Dutzi, A., Huber, W. and Libner, P.: On the parameters influencing air-water gas  
717 exchange, *J. Geophys. Res. Oceans*, 92(C2), 1937–1949, doi:10.1029/JC092iC02p01937, 1987.

718 Jarrell, K. F.: Extreme Oxygen Sensitivity in Methanogenic Archaeobacteria, *BioScience*, 35(5), 298–302,  
719 doi:10.2307/1309929, 1985.

720 Karl, D. M. and Tilbrook, B. D.: Production and transport of methane in oceanic particulate organic matter, *Nature*,  
721 368(6473), 732–734, doi:10.1038/368732a0, 1994.

722 Karl, D. M., Beversdorf, L., Björkman, K. M., Church, M. J., Martinez, A. and Delong, E. F.: Aerobic production of  
723 methane in the sea, *Nature Geosci.*, 1(7), 473–478, doi:10.1038/ngeo234, 2008.

724 Khatun, S., Iwata, T., Kojima, H., Fukui, M., Aoki, T., Mochizuki, S., Naito, A., Kobayashi, A. and Uzawa, R.: Aerobic  
725 methane production by planktonic microbes in lakes, *Science of The Total Environment*, 696, 133916,  
726 doi:10.1016/j.scitotenv.2019.133916, 2019.

727 Khatun, S., Iwata, T., Kojima, H., Ikarashi, Y., Yamanami, K., Imazawa, D., Kenta, T., Shinohara, R. and Saito, H.: Linking  
728 Stoichiometric Organic Carbon–Nitrogen Relationships to planktonic Cyanobacteria and Subsurface Methane  
729 Maximum in Deep Freshwater Lakes, *Water*, 12(2), 402, doi:10.3390/w12020402, 2020.

730 Kiene, R. P.: Production and consumption of methane in aquatic systems, *Microbial Production and Consumption of*  
731 *Greenhouse Gases: Methane, Nitrogen Oxides, and Halomethanes*, 1991.

- 732 Klintzsch, T., Langer, G., Nehrke, G., Wieland, A., Lenhart, K. and Keppler, F.: Methane production by three widespread  
733 marine phytoplankton species: release rates, precursor compounds, and potential relevance for the environment,  
734 *Biogeosciences*, 16(20), 4129–4144, doi:<https://doi.org/10.5194/bg-16-4129-2019>, 2019.
- 735 Lenhart, K., Bunge, M., Ratering, S., Neu, T. R., Schüttmann, I., Greule, M., Kammann, C., Schnell, S., Müller, C., Zorn, H.  
736 and Keppler, F.: Evidence for methane production by saprotrophic fungi, *Nat. Commun.*, 3, 1046,  
737 doi:10.1038/ncomms2049, 2012.
- 738 Lenhart, K., Althoff, F., Greule, M. and Keppler, F.: Technical Note: Methionine, a precursor of methane in living plants,  
739 *Biogeosciences*, 12(6), 1907–1914, doi:10.5194/bg-12-1907-2015, 2015.
- 740 Lenhart, K., Klintzsch, T., Langer, G., Nehrke, G., Bunge, M., Schnell, S. and Keppler, F.: Evidence for methane production  
741 by the marine algae *Emiliana huxleyi*, *Biogeosciences*, 13(10), 3163–3174, doi:10.5194/bg-13-3163-2016, 2016.
- 742 León-Palmero, E., Reche, I. and Morales-Baquero, R.: Atenuación de luz en embalses del sur-este de la Península Ibérica,  
743 *Ingeniería del agua*, 23(1), 65–75, doi:10.4995/ia.2019.10655, 2019.
- 744 León-Palmero, E., Morales-Baquero, R. and Reche, I.: Greenhouse gas fluxes from reservoirs determined by watershed  
745 lithology, morphometry, and anthropogenic pressure, *Environ. Res. Lett.*, 15(4), 044012, doi:10.1088/1748-  
746 9326/ab7467, 2020.
- 747 Liu, H., Jing, H., Wong, T. H. C. and Chen, B.: Co-occurrence of phycocyanin- and phycoerythrin-rich *Synechococcus* in  
748 subtropical estuarine and coastal waters of Hong Kong, *Environ. Microbiol. Rep.*, 6(1), 90–99, doi:10.1111/1758-  
749 2229.12111, 2014.
- 750 Marotta, H., Pinho, L., Gudas, C., Bastviken, D., Tranvik, L. J. and Enrich-Prast, A.: Greenhouse gas production in low-  
751 latitude lake sediments responds strongly to warming, *Nature Clim. Change*, 4(6), 467–470,  
752 doi:10.1038/nclimate2222, 2014.
- 753 Michmerhuizen, C. M., Striegl, R. G. and McDonald, M. E.: Potential methane emission from north-temperate lakes  
754 following ice melt, *Limnol. Oceanogr.*, 41(5), 985–991, doi:10.4319/lo.1996.41.5.0985, 1996.
- 755 Mitsch, W. J., Bernal, B., Nahlik, A. M., Mander, Ü., Zhang, L., Anderson, C. J., Jørgensen, S. E. and Brix, H.: Wetlands,  
756 carbon, and climate change, *Landsc. Ecol.*, 28(4), 583–597, doi:10.1007/s10980-012-9758-8, 2012.
- 757 Morris, D. P. and Lewis, W. M.: Phytoplankton nutrient limitation in Colorado mountain lakes, *Freshwater Biol.*, 20(3),  
758 315–327, doi:10.1111/j.1365-2427.1988.tb00457.x, 1988.
- 759 Mortimer, C. H.: The oxygen content of air-saturated fresh waters, and aids in calculating percentage saturation,  
760 Schweizerbart Science Publishers, Stuttgart, Germany. [online] Available from:  
761 [http://www.schweizerbart.de/publications/detail/isbn/9783510520060/Mitteilungen\\_IVL\\_Nr\\_6](http://www.schweizerbart.de/publications/detail/isbn/9783510520060/Mitteilungen_IVL_Nr_6), 1956.
- 762 Murase, J. and Sugimoto, A.: Inhibitory effect of light on methane oxidation in the pelagic water column of a mesotrophic  
763 lake (Lake Biwa, Japan), *Limnology and Oceanography*, 50(4), 1339–1343, doi:10.4319/lo.2005.50.4.1339, 2005.
- 764 Murase, J., Sakai, Y., Sugimoto, A., Okubo, K. and Sakamoto, M.: Sources of dissolved methane in Lake Biwa, *Limnology*,  
765 4(2), 91–99, doi:10.1007/s10201-003-0095-0, 2003.



- 766 Murphy, J. and Riley, J. P.: A modified single solution method for the determination of phosphate in natural waters, *Anal.*  
767 *Chim. Acta*, 27(Supplement C), 31–36, doi:10.1016/S0003-2670(00)88444-5, 1962.
- 768 Musenze, R. S., Grinham, A., Werner, U., Gale, D., Sturm, K., Udy, J. and Yuan, Z.: Assessing the spatial and temporal  
769 variability of diffusive methane and nitrous oxide emissions from subtropical freshwater reservoirs, *Environ. Sci.*  
770 *Technol.*, 48(24), 14499–14507, doi:10.1021/es505324h, 2014.
- 771 Naqvi, S. W. A., Lam, P., Narvenkar, G., Sarkar, A., Naik, H., Pratihary, A., Shenoy, D. M., Gauns, M., Kurian, S., Damare,  
772 S., Duret, M., Lavik, G. and Kuypers, M. M. M.: Methane stimulates massive nitrogen loss from freshwater reservoirs  
773 in India, *Nat. Commun.*, 9(1), 1–10, doi:10.1038/s41467-018-03607-z, 2018.
- 774 Odum, H. T.: Primary Production in Flowing Waters, *Limnol. Oceanogr.*, 1(2), 102–117, doi:10.4319/lo.1956.1.2.0102,  
775 1956.
- 776 Okuku, E. O., Bouillon, S., Tole, M. and Borges, A. V.: Diffusive emissions of methane and nitrous oxide from a cascade of  
777 tropical hydropower reservoirs in Kenya, *Lakes & Reservoirs: Research & Management*, 24(2), 127–135,  
778 doi:10.1111/lre.12264, 2019.
- 779 Oswald, K., Milucka, J., Brand, A., Littmann, S., Wehrli, B., Kuypers, M. M. M. and Schubert, C. J.: Light-Dependent  
780 Aerobic Methane Oxidation Reduces Methane Emissions from Seasonally Stratified Lakes, *PLOS ONE*, 10(7),  
781 doi:10.1371/journal.pone.0132574, 2015.
- 782 Oswald, K., Jegge, C., Tischer, J., Berg, J., Brand, A., Miracle, M. R., Soria, X., Vicente, E., Lehmann, M. F., Zopfi, J. and  
783 Schubert, C. J.: Methanotrophy under Versatile Conditions in the Water Column of the Ferruginous Meromictic Lake  
784 La Cruz (Spain), *Front. Microbiol.*, 7, doi:10.3389/fmicb.2016.01762, 2016.
- 785 Owens, N. J. P., Law, C. S., Mantoura, R. F. C., Burkill, P. H. and Llewellyn, C. A.: Methane flux to the atmosphere from  
786 the Arabian Sea, *Nature*, 354(6351), 293–296, doi:10.1038/354293a0, 1991.
- 787 Peeters, F., Wüest, A., Piepke, G. and Imboden, D. M.: Horizontal mixing in lakes, *J. Geophys. Res. Oceans*, 101(C8),  
788 18361–18375, doi:10.1029/96JC01145, 1996.
- 789 Peeters, F., Fernandez Encinas, J. and Hofmann, H.: Sediment fluxes rather than oxic methanogenesis explain diffusive CH<sub>4</sub>  
790 emissions from lakes and reservoirs, *Sci. Rep.*, 9(1), 1–10, doi:10.1038/s41598-018-36530-w, 2019.
- 791 R Core Team: R: A Language and Environment for Statistical Computing, R Foundation for Statistical Computing, Vienna,  
792 Austria. [online] Available from: <http://www.R-project.org/>, 2014.
- 793 Rasilo, T., Prairie, Y. T. and del Giorgio, P. A.: Large-scale patterns in summer diffusive CH<sub>4</sub> fluxes across boreal lakes, and  
794 contribution to diffusive C emissions, *Glob. Change Biol.*, 21(3), 1124–1139, doi:10.1111/gcb.12741, 2015.
- 795 Repeta, D. J., Ferrón, S., Sosa, O. A., Johnson, C. G., Repeta, L. D., Acker, M., DeLong, E. F. and Karl, D. M.: Marine  
796 methane paradox explained by bacterial degradation of dissolved organic matter, *Nat. Geosci.*, 9(12), 884–887,  
797 doi:10.1038/ngeo2837, 2016.
- 798 Reynolds, C. S.: Phytoplankton periodicity: the interactions of form, function and environmental variability, *Freshwater*  
799 *Biology*, 14(2), 111–142, doi:10.1111/j.1365-2427.1984.tb00027.x, 1984.

- 800 Roland, F. A. E., Darchambeau, F., Morana, C. and Borges, A. V.: Nitrous oxide and methane seasonal variability in the  
801 epilimnion of a large tropical meromictic lake (Lake Kivu, East-Africa), *Aquat. Sci.*, 79(2), 209–218,  
802 doi:10.1007/s00027-016-0491-2, 2017.
- 803 Rudd, J. W. M. and Hamilton, R. D.: Methane cycling in a eutrophic shield lake and its effects on whole lake metabolism,  
804 *Limnol. Oceanogr.*, 23(2), 337–348, doi:10.4319/lo.1978.23.2.0337, 1978.
- 805 Sabo, E., Roy, D., Hamilton, P. B., Hehanussa, P. E., McNeely, R. and Haffner, G. D.: The plankton community of Lake  
806 Matano: factors regulating plankton composition and relative abundance in an ancient, tropical lake of Indonesia, in  
807 *Patterns and Processes of Speciation in Ancient Lakes*, pp. 225–235, Springer., 2008.
- 808 Saunio, M., Bousquet, P., Poulter, B., Peregon, A., Ciais, P., Canadell, J. G., Dlugokencky, E. J., Etiope, G., Bastviken, D.,  
809 Houweling, S., Janssens-Maenhout, G., Tubiello, F. N., Castaldi, S., Jackson, R. B., Alexe, M., Arora, V. K.,  
810 Beerling, D. J., Bergamaschi, P., Blake, D. R., Brailsford, G., Brovkin, V., Bruhwiler, L., Crevoisier, C., Crill, P.,  
811 Covey, K., Curry, C., Frankenberg, C., Gedney, N., Höglund-Isaksson, L., Ishizawa, M., Ito, A., Joos, F., Kim, H.-S.,  
812 Kleinen, T., Krummel, P., Lamarque, J.-F., Langenfelds, R., Locatelli, R., Machida, T., Maksyutov, S., McDonald, K.  
813 C., Marshall, J., Melton, J. R., Morino, I., Naik, V., O’Doherty, S., Parmentier, F.-J., Patra, P. K., Peng, C., Peng, S.,  
814 Peters, G. P., Pison, I., Prigent, C., Prinn, R., Ramonet, M., Riley, W. J., Saito, M., Santini, M., Schroeder, R.,  
815 Simpson, I. J., Spahni, R., Steele, P., Takizawa, A., Thornton, B. F., Tian, H., Tohjima, Y., Viovy, N., Voulgarakis,  
816 A., van Weele, M., van der Werf, G. R., Weiss, R., Wiedinmyer, C., Wilton, D. J., Wiltshire, A., Worthy, D., Wunch,  
817 D., Xu, X., Yoshida, Y., Zhang, B., Zhang, Z. and Zhu, Q.: The global methane budget 2000–2012, *Earth Syst. Sci.*  
818 *Data*, 8, 697–751, 2016.
- 819 Schlesinger, W. H. and Bernhardt, E. S.: *Biogeochemistry: An Analysis of Global Change*, Academic Press., 2013.
- 820 Schmale, O., Wäge, J., Mohrholz, V., Wasmund, N., Gräwe, U., Rehder, G., Labrenz, M. and Loick-Wilde, N.: The  
821 contribution of zooplankton to methane supersaturation in the oxygenated upper waters of the central Baltic Sea,  
822 *Limnol. Oceanogr.*, 63(1), 412–430, doi:10.1002/lno.10640, 2018.
- 823 Schmidt, U. and Conrad, R.: Hydrogen, carbon monoxide, and methane dynamics in Lake Constance, *Limnol. Oceanogr.*,  
824 38(6), 1214–1226, doi:10.4319/lo.1993.38.6.1214, 1993.
- 825 Schubert, C. J. and Wehrli, B.: Contribution of Methane Formation and Methane Oxidation to Methane Emission from  
826 Freshwater Systems, in *Biogenesis of Hydrocarbons*, edited by A. J. M. Stams and D. Sousa, pp. 1–31, Springer  
827 International Publishing, Cham., 2018.
- 828 Schulz, M., Faber, E., Hollerbach, A., Schröder, H. G. and Güde, H.: The methane cycle in the epilimnion of Lake  
829 Constance, *Archiv für Hydrobiologie*, 157–176, doi:10.1127/archiv-hydrobiol/151/2001/157, 2001.
- 830 Schwarz, J. I. K., Eckert, W. and Conrad, R.: Response of the methanogenic microbial community of a profundal lake  
831 sediment (Lake Kinneret, Israel) to algal deposition, *Limnol. Oceanogr.*, 53(1), 113–121,  
832 doi:10.4319/lo.2008.53.1.0113, 2008.
- 833 Scranton, M. I. and Brewer, P. G.: Occurrence of methane in the near-surface waters of the western subtropical North-

834 Atlantic, *Deep-Sea Res.*, 24(2), 127–138, doi:10.1016/0146-6291(77)90548-3, 1977.

835 Segers, R.: Methane production and methane consumption: a review of processes underlying wetland methane fluxes,  
836 *Biogeochemistry*, 41(1), 23–51, doi:10.1023/A:1005929032764, 1998.

837 Sepulveda-Jauregui, A., Hoyos-Santillan, J., Martinez-Cruz, K., Walter Anthony, K. M., Casper, P., Belmonte-Izquierdo, Y.  
838 and Thalasso, F.: Eutrophication exacerbates the impact of climate warming on lake methane emission, *Sci. Total*  
839 *Environ.*, 636, 411–419, doi:10.1016/j.scitotenv.2018.04.283, 2018.

840 Seweryn, P., Van, L. B., Kjeldgaard, M., Russo, C. J., Passmore, L. A., Hove-Jensen, B., Jochimsen, B. and Brodersen, D.  
841 E.: Structural insights into the bacterial carbon-phosphorus lyase machinery, *Nature*, 525(7567), 68–72,  
842 doi:10.1038/nature14683, 2015.

843 Shaw, S. L., Chisholm, S. W. and Prinn, R. G.: Isoprene production by *Prochlorococcus*, a marine cyanobacterium, and other  
844 phytoplankton, *Mar. Chem.*, 80(4), 227–245, doi:10.1016/S0304-4203(02)00101-9, 2003.

845 Sierra, A., Jiménez-López, D., Ortega, T., Ponce, R., Bellanco, M. J., Sánchez-Leal, R., Gómez-Parra, A. and Forja, J.:  
846 Spatial and seasonal variability of CH<sub>4</sub> in the eastern Gulf of Cadiz (SW Iberian Peninsula), *Sci. Total Environ.*, 590–  
847 591, 695–707, doi:10.1016/j.scitotenv.2017.03.030, 2017.

848 Staehr, P. A., Bade, D., Bogert, M. C. V. de, Koch, G. R., Williamson, C., Hanson, P., Cole, J. J. and Kratz, T.: Lake  
849 metabolism and the diel oxygen technique: State of the science, *Limnol. Oceanogr. Methods*, 8(11), 628–644,  
850 doi:10.4319/lom.2010.8.0628, 2010.

851 Steinke, M., Hodapp, B., Subhan, R., Bell, T. G. and Martin-Creuzburg, D.: Flux of the biogenic volatiles isoprene and  
852 dimethyl sulfide from an oligotrophic lake, *Sci. Rep.*, 8(1), 1–10, doi:10.1038/s41598-017-18923-5, 2018.

853 Tang, K. W., McGinnis, D. F., Frindte, K., Brüchert, V. and Grossart, H.-P.: Paradox reconsidered: Methane oversaturation  
854 in well-oxygenated lake waters, *Limnol. Oceanogr.*, 59(1), 275–284, doi:10.4319/lo.2014.59.1.0275, 2014.

855 Tang, K. W., McGinnis, D. F., Ionescu, D. and Grossart, H.-P.: Methane Production in Oxidic Lake Waters Potentially  
856 Increases Aquatic Methane Flux to Air, *Environ. Sci. Technol. Lett.*, 3(6), 227–233, doi:10.1021/acs.estlett.6b00150,  
857 2016.

858 Teikari, J. E., Fewer, D. P., Shrestha, R., Hou, S., Leikoski, N., Mäkelä, M., Simojoki, A., Hess, W. R. and Sivonen, K.:  
859 Strains of the toxic and bloom-forming *Nodularia spumigena* (cyanobacteria) can degrade methylphosphonate and  
860 release methane, *ISME J.*, 12(6), 1619–1630, doi:10.1038/s41396-018-0056-6, 2018.

861 Thalasso, F., Sepulveda-Jauregui, A., Gandois, L., Martinez-Cruz, K., Gerardo-Nieto, O., Astorga-España, M. S.,  
862 Teisserenc, R., Lavergne, C., Tananaev, N., Barret, M. and Cabrol, L.: Sub-oxycline methane oxidation can fully  
863 uptake CH<sub>4</sub> produced in sediments: case study of a lake in Siberia, *Sci. Rep.*, 10(1), 1–7, doi:10.1038/s41598-020-  
864 60394-8, 2020.

865 Thanh-Duc, N., Crill, P. and Bastviken, D.: Implications of temperature and sediment characteristics on methane formation  
866 and oxidation in lake sediments, *Biogeochemistry*, 100(1), 185–196, doi:10.1007/s10533-010-9415-8, 2010.

867 Tilbrook, B. D. and Karl, D. M.: Methane sources, distributions and sinks from California coastal waters to the oligotrophic

868 North Pacific gyre, *Mar. Chem.*, 49(1), 51–64, doi:10.1016/0304-4203(94)00058-L, 1995.

869 del Valle, D. A. and Karl, D. M.: Aerobic production of methane from dissolved water-column methylphosphonate and  
870 sinking particles in the North Pacific Subtropical Gyre, *Aquat. Microb. Ecol.*, 73(2), 93–105, doi:10.3354/ame01714,  
871 2014.

872 Wang, Q., Dore, J. E. and McDermott, T. R.: Methylphosphonate metabolism by *Pseudomonas* sp. populations contributes to  
873 the methane oversaturation paradox in an oxic freshwater lake, *Environ. Microbiol.*, 19(6), 2366–2378,  
874 doi:10.1111/1462-2920.13747, 2017.

875 West, W. E., Coloso, J. J. and Jones, S. E.: Effects of algal and terrestrial carbon on methane production rates and  
876 methanogen community structure in a temperate lake sediment, *Freshwater Biol.*, 57(5), 949–955,  
877 doi:10.1111/j.1365-2427.2012.02755.x, 2012.

878 West, W. E., McCarthy, S. M. and Jones, S. E.: Phytoplankton lipid content influences freshwater lake methanogenesis,  
879 *Freshwater Biol.*, 60(11), 2261–2269, doi:10.1111/fwb.12652, 2015.

880 West, W. E., Creamer, K. P. and Jones, S. E.: Productivity and depth regulate lake contributions to atmospheric methane:  
881 Lake productivity fuels methane emissions, *Limnol. Oceanogr.*, 61(S1), S51–S61, doi:10.1002/lno.10247, 2016.

882 White, A. K. and Metcalf, W. W.: Microbial Metabolism of Reduced Phosphorus Compounds, *Annu. Rev. Microbiol.*, 61(1),  
883 379–400, doi:10.1146/annurev.micro.61.080706.093357, 2007.

884 Wiesenburg, D. A. and Guinasso, N. L.: Equilibrium solubilities of methane, carbon monoxide, and hydrogen in water and  
885 sea water, *J. Chem. Eng. Data*, 24(4), 356–360, doi:10.1021/je60083a006, 1979.

886 Willén, E.: Phytoplankton and reversed Eutrophication in Lake Mälaren, Central Sweden, 1965–1983, *Br. Phycol. J.*, 22(2),  
887 193–208, doi:10.1080/00071618700650241, 1987.

888 Wood, S. N.: Generalized additive models: an introduction with R, Chapman and Hall/CRC, New York, USA., 2006.

889 Wood, S. N.: Fast stable restricted maximum likelihood and marginal likelihood estimation of semiparametric generalized  
890 linear models, *J. R. Stat. Soc. Series B Stat. Methodol.*, 73(1), 3–36, doi:10.1111/j.1467-9868.2010.00749.x, 2011.

891 Yamamoto, S., Alcauskas, J. B. and Crozier, T. E.: Solubility of methane in distilled water and seawater, *J. Chem. Eng.*  
892 *Data*, 21(1), 78–80, doi:10.1021/je60068a029, 1976.

893 Yao, M., Henny, C. and Maresca, J. A.: Freshwater bacteria release methane as a byproduct of phosphorus acquisition, *Appl.*  
894 *Environ. Microbiol.*, 82(23), 6994–7003, doi:10.1128/AEM.02399-16, 2016a.

895 Yao, M., Elling, F. J., Jones, C., Nomosatryo, S., Long, C. P., Crowe, S. A., Antoniewicz, M. R., Hinrichs, K.-U. and  
896 Maresca, J. A.: Heterotrophic bacteria from an extremely phosphate-poor lake have conditionally reduced phosphorus  
897 demand and utilize diverse sources of phosphorus, *Environ. Microbiol.*, 18(2), 656–667, doi:10.1111/1462-  
898 2920.13063, 2016b.

899 Yoch, D. C.: Dimethylsulfoniopropionate: its sources, role in the marine food web, and biological degradation to  
900 dimethylsulfide, *Appl. Environ. Microbiol.*, 68(12), 5804–5815, doi:10.1128/AEM.68.12.5804-5815.2002, 2002.

901 Yvon-Durocher, G., Allen, A. P., Bastviken, D., Conrad, R., Gudas, C., St-Pierre, A., Thanh-Duc, N. and del Giorgio, P.

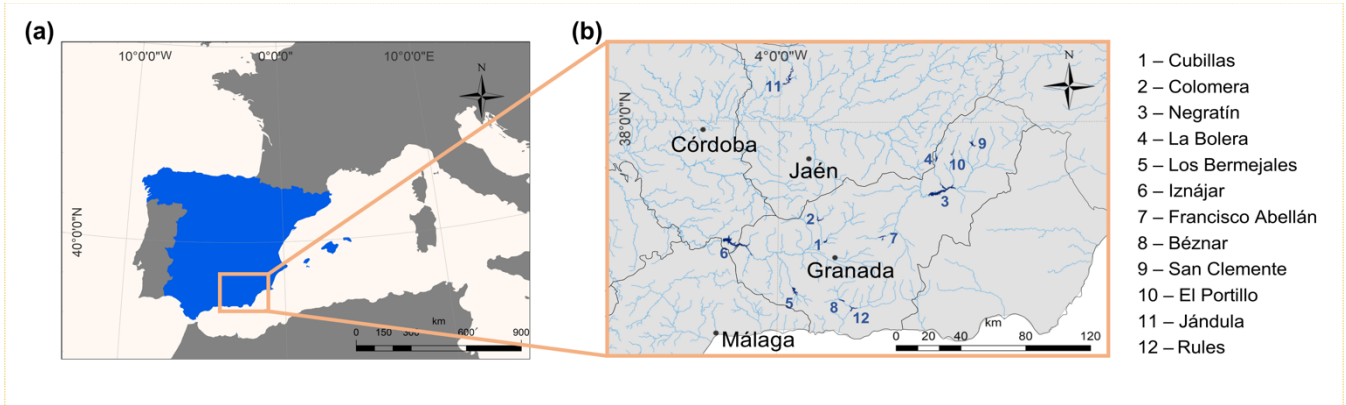
902 A.: Methane fluxes show consistent temperature dependence across microbial to ecosystem scales, *Nature*,  
903 507(7493), 488–491, doi:10.1038/nature13164, 2014.

904 Zindler, C., Bracher, A., Marandino, C. A., Taylor, B., Torrecilla, E., Kock, A. and Bange, H. W.: Sulphur compounds,  
905 methane, and phytoplankton: interactions along a north–south transit in the western Pacific Ocean, *Biogeosciences*,  
906 10(5), 3297–3311, doi:10.5194/bg-10-3297-2013, 2013.

907

908

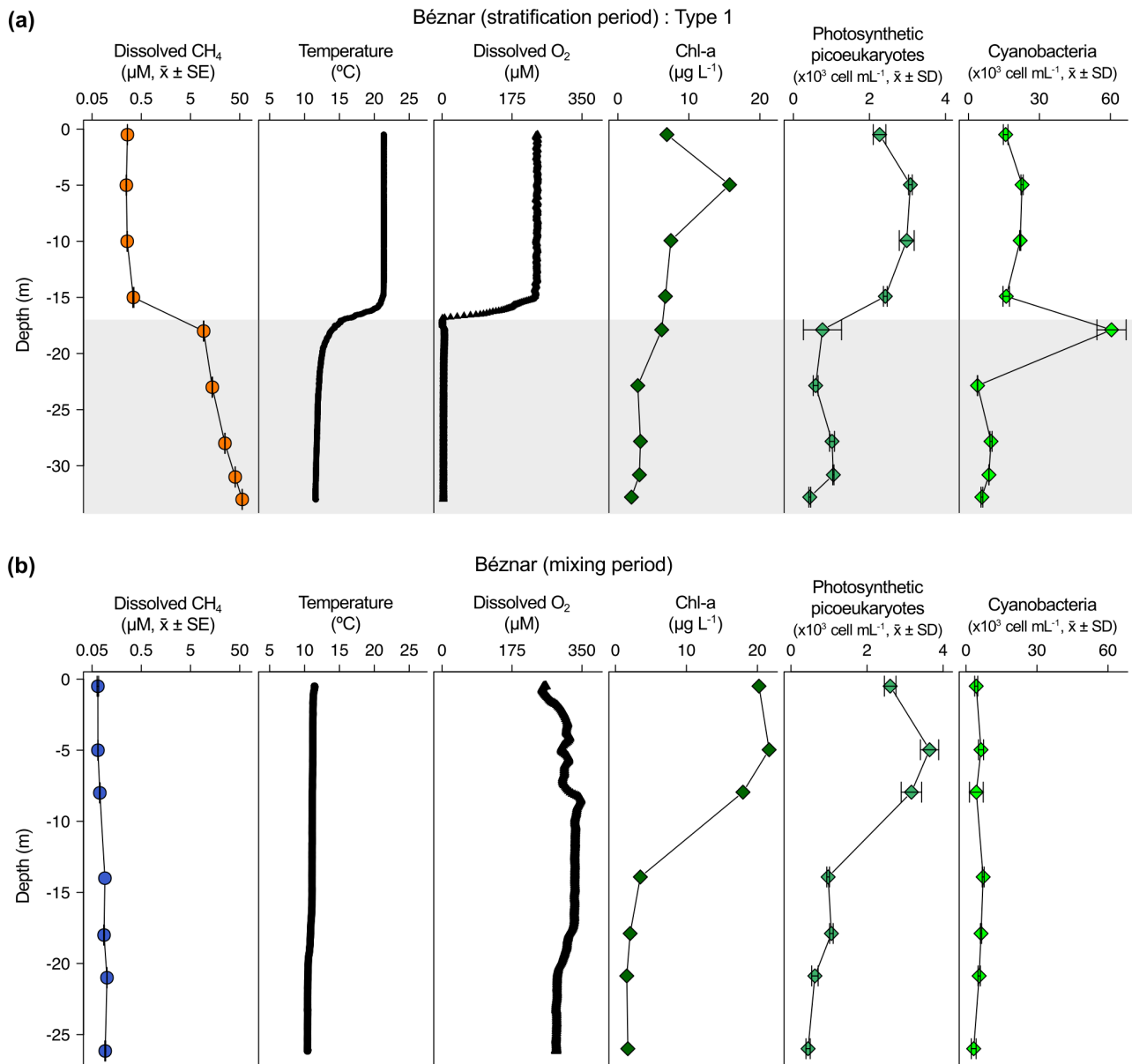
909  
910



911

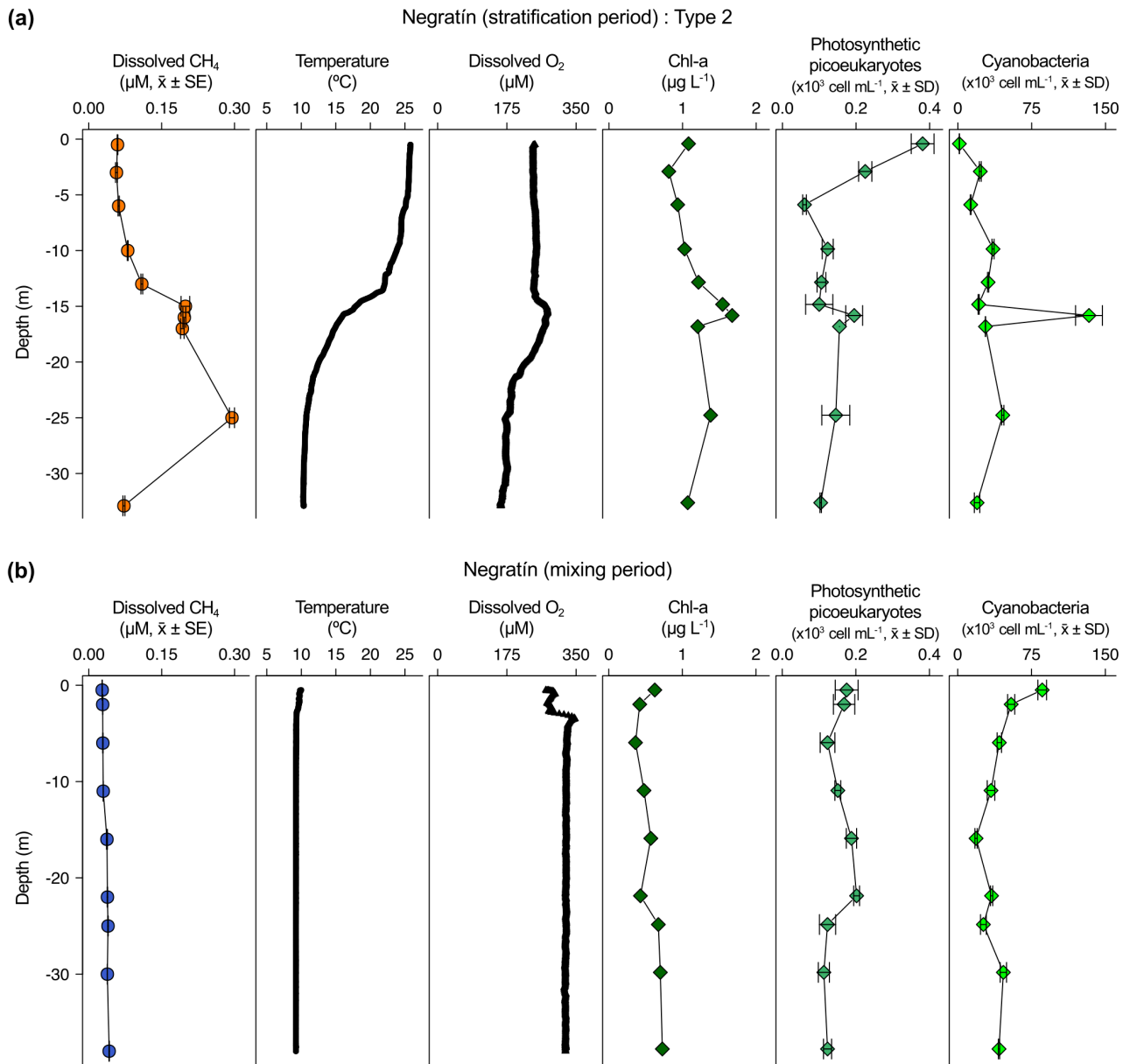
912 **Figure 1: Geographical location of the study reservoirs.** (a) The location area of the study reservoirs is delimited by an orange box in  
913 the South of the Iberian Peninsula. (b) Detailed location of the twelve reservoirs with the numbers (#1–12) and their corresponding names  
914 listed on the side. Geographical coordinates appear in Table 1. We obtained these maps using ArcGIS® 10.2 software (ESRI, 2012) under  
915 the Universidad de Granada license. ESRI: ArcGIS, Redlands, CA.

916



917

918 **Figure 2: Vertical profiles of physicochemical and biological variables in Béznař reservoir.** Dissolved methane concentration ( $\text{CH}_4$ ,  
 919  $\mu\text{M}$ , mean  $\pm$  standard error), temperature ( $^{\circ}\text{C}$ ), dissolved oxygen concentration ( $\text{DO}$ ,  $\mu\text{M}$ ), chlorophyll-a concentration ( $\text{Chl-a}$ ,  $\mu\text{g L}^{-1}$ ),  
 920 abundance of photosynthetic picoeukaryotes ( $\times 10^3 \text{ cell mL}^{-1}$ , mean  $\pm$  standard deviation) and abundance of cyanobacteria ( $\times 10^3 \text{ cell mL}^{-1}$ ,  
 921 mean  $\pm$  standard deviation) during the stratification period **(a)** and the mixing period **(b)**. The grey area represents the anoxic zone ( $\text{DO} < 7.5 \mu\text{M}$ ). Note the logarithmic scales in the x-axis of the dissolved  $\text{CH}_4$  profiles. The sampling for the stratification period was on October  
 922 7, 2016 and February 23, 2017 for the mixing period.  
 923  
 924

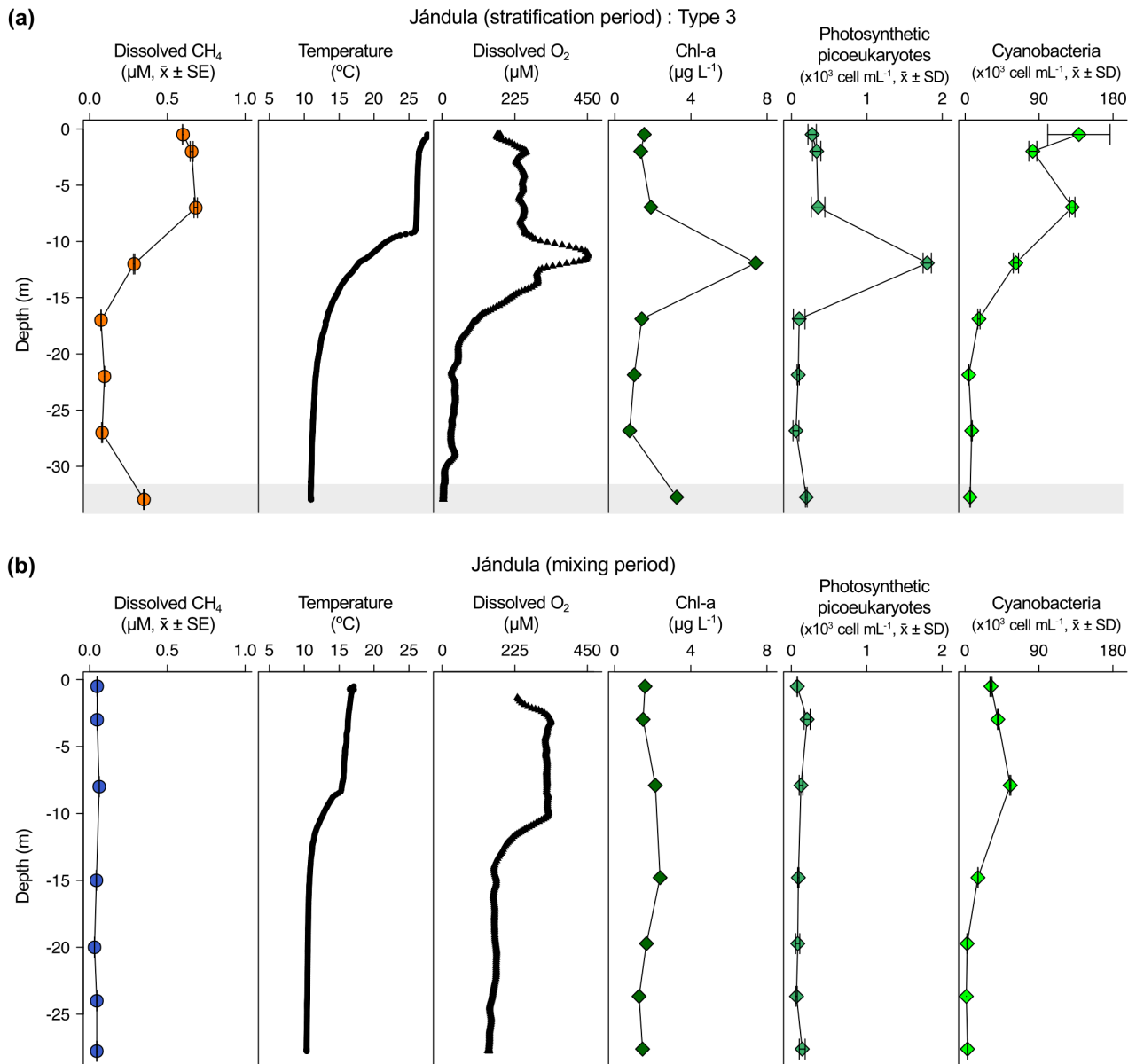


925

926 **Figure 3: Vertical profiles of physicochemical and biological variables in Negrátin reservoir.** Dissolved methane concentration (CH<sub>4</sub>,  
 927 μM, mean ± standard error), temperature (°C), dissolved oxygen concentration (DO, μM), chlorophyll-a concentration (Chl-a, μg L<sup>-1</sup>),  
 928 abundance of photosynthetic picoeukaryotes (x10<sup>3</sup> cell mL<sup>-1</sup>, mean ± standard deviation) and abundance of cyanobacteria (x10<sup>3</sup> cell mL<sup>-1</sup>,  
 929 mean ± standard deviation) during the stratification period (a) and the mixing period (b). The sampling for the stratification period was on  
 930 July 27, 2016 and February 16, 2017 for the mixing period.

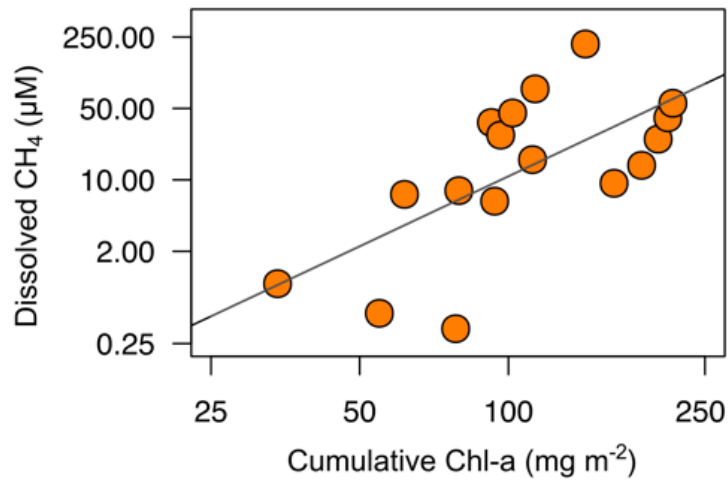
931





932

933 **Figure 4: Vertical profiles of physicochemical and biological variables in Jándula reservoir.** Dissolved methane concentration ( $\text{CH}_4$ ,  
 934  $\mu\text{M}$ , mean  $\pm$  standard error), temperature ( $^\circ\text{C}$ ), dissolved oxygen concentration (DO,  $\mu\text{M}$ ), chlorophyll-a concentration (Chl-a,  $\mu\text{g L}^{-1}$ ),  
 935 abundance of photosynthetic picoeukaryotes ( $\times 10^3 \text{ cell mL}^{-1}$ , mean  $\pm$  standard deviation) and abundance of cyanobacteria ( $\times 10^3 \text{ cell mL}^{-1}$ ,  
 936 mean  $\pm$  standard deviation) during the stratification period (a) and the mixing period (b). The grey area represents the anoxic zone (DO <  
 937  $7.5 \mu\text{M}$ ). The sampling for the stratification period was on July 24, 2017 and April 5, 2017 for the mixing period.

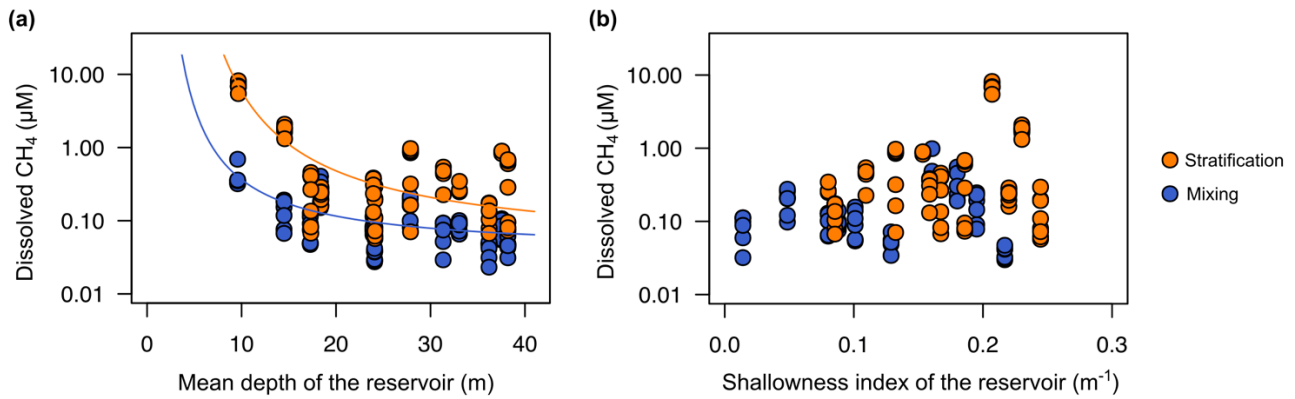


938

939 **Figure 5:** Power relationship between the depth-cumulative chlorophyll-a concentration and the concentration of dissolved CH<sub>4</sub> in the  
 940 anoxic waters during the stratification period ( $\text{CH}_4, \mu\text{M} = 3.0 \cdot 10^{-4} \text{ Cumulative Chl-a}^{2.28}$ ,  $n=17$ ,  $\text{adj } R^2 = 0.40$ ). Note that both axes are in  
 941 logarithmic scale. More statistical details in Table S2.

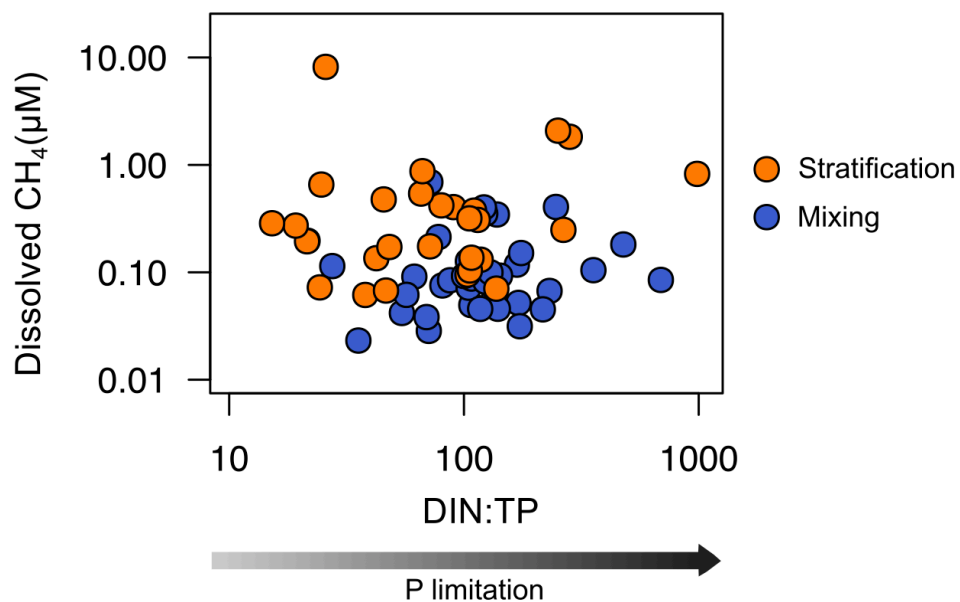
942

943



944

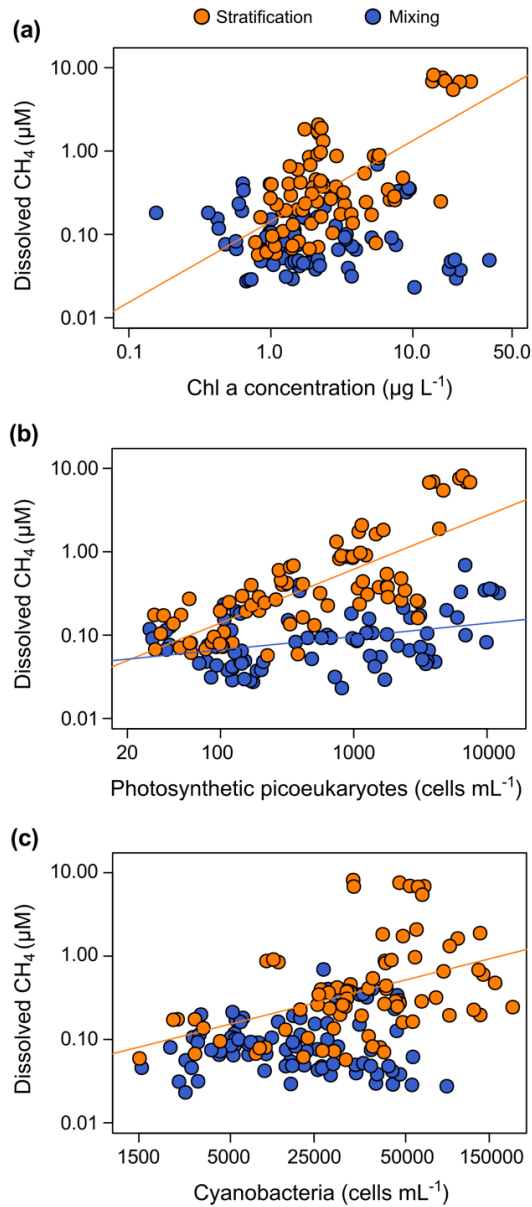
945 **Figure 6: Reservoir morphometry and the dissolved CH<sub>4</sub> concentration in the oxic zone.** (a) Exponential decay relationships of the  
 946 dissolved CH<sub>4</sub> concentration and the mean depth (m) during the stratification period ( $\text{CH}_4 = 4.0 \cdot 10^{-2} e^{(50.0/\text{mean depth})}$ ,  $n=78$ ,  $\text{adj } R^2 = 0.95$ )  
 947 and the mixing period ( $\text{CH}_4 = 3.7 \cdot 10^{-2} e^{(22.9/\text{mean depth})}$ ,  $n=82$ ,  $\text{adj } R^2 = 0.54$ ). (b) Scatterplot of dissolved CH<sub>4</sub> concentration and the  
 948 reservoir shallowness index during the stratification period ( $p\text{-value} = 0.134$ ) and the mixing period ( $n=0.114$ ). More statistical details in  
 949 Table S2.



950

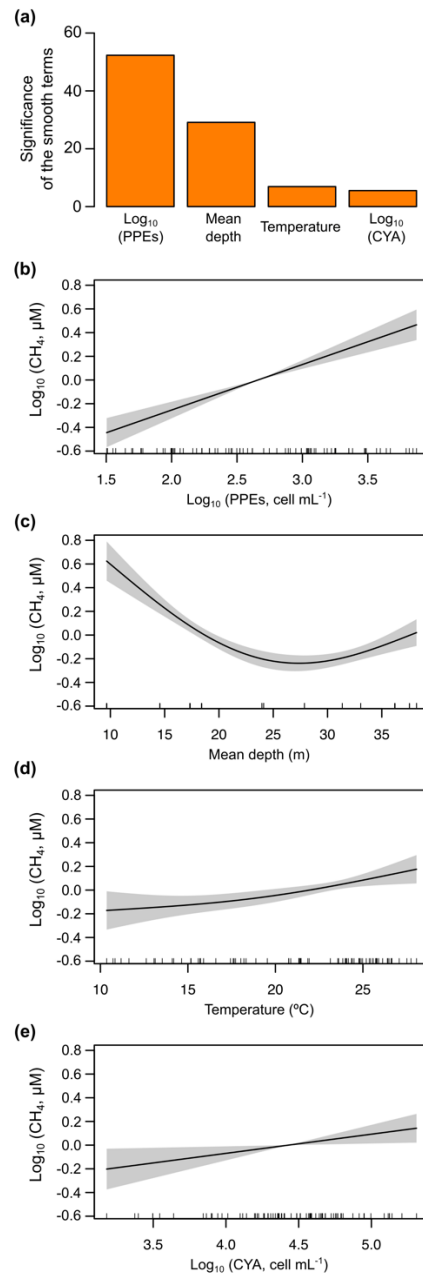
951 **Figure 7: Phosphorus limitation and the dissolved CH<sub>4</sub> concentration in the oxic waters.** Scatterplot of dissolved CH<sub>4</sub> concentration  
 952 and the ration between dissolved inorganic nitrogen (DIN) and the total phosphorus (TP) (μmol N : μmol P). Note the logarithmic scale in  
 953 both axes.

954



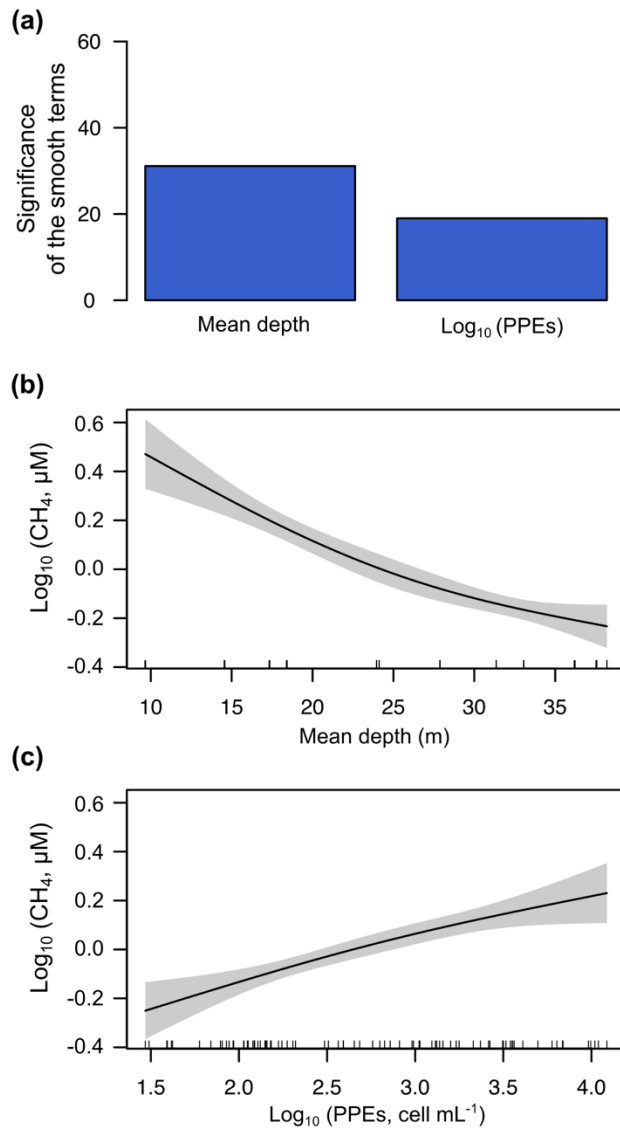
955

956 **Figure 8: Phytoplanktonic variable coupled with the dissolved CH<sub>4</sub> concentration in the oxic waters.** (a) The dissolved CH<sub>4</sub>  
 957 concentration was significantly related to the chlorophyll-a concentration during the stratification period (p-value <0.001), but they were  
 958 not related during the mixing period (p-value = 0.469). The relationship during the stratification period was a power function (CH<sub>4</sub>, µM =  
 959 0.14 Chl-a<sup>0.97</sup>; n = 78, adj R<sup>2</sup>=0.40) (b) Relationships between dissolved CH<sub>4</sub> concentration and the abundance of photosynthetic  
 960 picoeukaryotes (PPEs) during the stratification period (CH<sub>4</sub>, µM = 7.2 · 10<sup>-3</sup> PPEs<sup>0.65</sup>; n = 78, adj R<sup>2</sup>=0.55, p-value <0.001) and the mixing  
 961 period (CH<sub>4</sub>, µM = 3.2 · 10<sup>-2</sup> PPEs<sup>0.16</sup>; n = 82, adj R<sup>2</sup>=0.12, p-value <0.001). (c) Relationship between dissolved CH<sub>4</sub> concentration and the  
 962 cyanobacteria abundance (CYA, cell mL<sup>-1</sup>). A power function described the relationship between the dissolved CH<sub>4</sub> and the CYA during  
 963 the stratification period (CH<sub>4</sub>, µM = 1.7 · 10<sup>-3</sup> CYA<sup>0.53</sup>; n = 78, adj R<sup>2</sup>=0.17, p-value <0.001). The relationship was not significant during  
 964 the mixing period (p-value = 0.666).



966

967 **Figure 9. Results of the Generalized Additive Model (GAM) fitted for the concentration of dissolved  $\text{CH}_4$  in the oxic waters during**  
 968 **the stratification period. (a)** Bar plot showing the significance of the smooth terms from the fitted GAM model (F values). **(b-e)** Partial  
 969 response plots from the fitted GAM model showing the additive effects of the covariates on the dissolved  $\text{CH}_4$  concentration: the  
 970 photosynthetic picoeukaryotes abundance ( $\text{log}_{10}$  PPEs) **(b)**, the mean depth **(c)**, the cyanobacteria abundance ( $\text{log}_{10}$  CYA) **(d)**, and water  
 971 temperature **(e)**. In partial response plots, the lines are the smoothing functions and the shaded areas represent 95% point-wise confidence  
 972 intervals. Rugs on x-axis indicate the distribution of the data. More details are provided in Table S3.



973

974 **Figure 10. Results of the Generalized Additive Model (GAM) fitted for the concentrations of CH<sub>4</sub> in the oxic waters during the**  
 975 **mixing period. (a)** Bar plot showing the significance of the smooth terms from the fitted GAM model (F values). **(b)** and **(c)** Partial  
 976 response plots from the fitted GAM model showing the additive effects of the covariates on the dissolved CH<sub>4</sub> concentration: the mean  
 977 depth **(b)** and the abundance of photosynthetic picoeukaryotes (log<sub>10</sub> PPEs) **(c)**. In partial response plots, the lines are the smoothing  
 978 functions and the shaded areas represent 95% point-wise confidence intervals. Rugs on x-axis indicate the distribution of the data. More  
 979 details are provided in Table S3.

980

981

982 **Table 1.** Geographical location and morphometric description of the study reservoirs.

Reservoir	Latitude (°, decimal degrees)	Longitude (°, decimal degrees)	Altitude (m)	Construction year	Reservoir area (km <sup>2</sup> )	Reservoir capacity (hm <sup>3</sup> )	Mean depth (m)	Shoreline development index (D <sub>L</sub> )	Shallowness index (m <sup>-1</sup> )
Cubillas	37.27	-3.68	640	1956	1.94	18.74	9.66	2.00	0.21
Colomera	37.40	-3.72	810	1990	2.76	40.18	14.56	3.35	0.23
Negratín	37.56	-2.95	618	1984	23.51	567.12	24.12	5.90	0.24
La Bolera	37.76	-2.90	950	1967	2.89	53.19	18.40	4.05	0.22
Los Bermejales	36.99	-3.89	852	1958	5.95	103.12	17.33	2.90	0.17
Iznájar	37.26	-4.33	425	1969	26.13	981.12	37.55	5.76	0.15
Francisco Abellán	37.31	-3.27	942	1991	2.43	58.21	23.95	3.80	0.16
Béznar	36.92	-3.55	486	1986	1.60	52.90	33.06	2.65	0.08
San Clemente	37.86	-2.65	1050	1990	3.76	117.92	31.36	3.43	0.11
El Portillo	37.81	-2.79	920	1999	1.18	32.90	27.88	3.69	0.13
Jándula	38.23	-3.97	350	1932	8.43	321.99	38.20	7.10	0.19
Rules	36.86	-3.49	239	2003	3.06	110.78	36.20	3.09	0.09

983

984

986 **Table 2.** Sampling date, depth of the mixing layer (m), and mean values of the DOC, TN, and TP concentrations, DIN:TP  
 987 ratio, and chlorophyll-a concentration in the water column of the study reservoirs during the stratification and the mixing  
 988 period. The depth of the mixing layer was inferred from the temperature profile.

Reservoir	Period	Sampling Date	DOC ( $\mu\text{M-C}$ )	TN ( $\mu\text{M-N}$ )	TP ( $\mu\text{M-P}$ )	DIN:TP ( $\mu\text{mol-N}:\mu\text{mol-P}$ )	Chl-a ( $\mu\text{g L}^{-1}$ )
Cubillas	Stratification	July 15, 2016	172.1	60.4	1.84	26	17.8
	Mixing	February 6, 2017	240.5	97.4	0.78	111	8.4
Colomera	Stratification	July 22, 2016	99.4	181.4	0.78	240	2.1
	Mixing	March 7, 2017	123.3	112.5	0.44	292	0.5
Negratín	Stratification	June 27, 2016	109.7	21.2	0.80	28	1.2
	Mixing	February 16, 2017	148.9	19.7	0.24	65	7.7
La Bolera	Stratification	June 28, 2016	123.7	17.3	0.61	25	2.0
	Mixing	April 8, 2017	107.4	34.4	0.15	178	0.8
Los Bermejales	Stratification	September 7, 2016	94.2	30.4	0.42	65	1.8
	Mixing	March 17, 2017	101.5	30.6	0.31	89	13.1
Iznájar	Stratification	September 9, 2016	116.8	278.5	0.39	729	5.1
	Mixing	March 15, 2017	147.5	260.0	1.16	393	1.1
Francisco Abellán	Stratification	September 28, 2016	90.6	27.8	0.28	200	1.9
	Mixing	March 21, 2017	118.0	28.5	0.47	63	1.1
Béznar	Stratification	October 7, 2016	74.3	74.2	0.68	227	6.0
	Mixing	February 23, 2017	121.6	105.6	0.95	104	3.7
San Clemente	Stratification	July 17, 2017	104.1	32.0	0.39	65	3.5
	Mixing	March 28, 2017	119.4	35.9	0.21	145	1.1
El Portillo	Stratification	July 18, 2017	78.0	22.8	0.17	102	2.4
	Mixing	March 30, 2017	76.4	34.4	0.26	109	1.7
Jándula	Stratification	July 24, 2017	359.9	34.3	0.78	43	2.3
	Mixing	April 5, 2017	399.4	46.2	0.37	104	1.2
Rules	Stratification	July 10, 2017	81.2	23.2	0.21	83	3.7
	Mixing	April 7, 2017	68.5	38.0	0.43	142	3.3



991

992 **Table 3.** Equations for the relationships between the phytoplanktonic variables and the dissolved CH<sub>4</sub> concentration in the  
 993 oxic waters. n.m. = not measured.

Driver	Period	n	Equation	Adj. R <sup>2</sup>	p-value
Chl-a concentration (µg L <sup>-1</sup> )	Stratification + Mixing	160	CH <sub>4</sub> (µM) = 0.12 Chl-a <sup>0.44</sup>	0.11	< 0.001
	Stratification	78	CH <sub>4</sub> (µM) = 0.14 Chl-a <sup>0.97</sup>	0.40	< 0.001
	Mixing	82	Not significantly related		0.469
Gross primary production (GPP, g O <sub>2</sub> m <sup>-3</sup> d <sup>-1</sup> )	Stratification	12	Marginally significant		0.077
	Mixing	n.m.			
Net ecosystem production (NEP, g O <sub>2</sub> m <sup>-3</sup> d <sup>-1</sup> )	Stratification	12	Not significantly related		0.536
	Mixing	n.m.			
Photosynthetic picoeukaryotes abundance (PPEs, cell mL <sup>-1</sup> )	Stratification + Mixing	160	CH <sub>4</sub> (µM) = 2.0·10 <sup>-2</sup> PPEs <sup>0.35</sup>	0.19	< 0.001
	Stratification	78	CH <sub>4</sub> (µM) = 7.2·10 <sup>-3</sup> PPEs <sup>0.65</sup>	0.57	< 0.001
	Mixing	82	CH <sub>4</sub> (µM) = 3.2·10 <sup>-2</sup> PPEs <sup>0.16</sup>	0.12	< 0.001
Cyanobacteria abundance (CYA, cell mL <sup>-1</sup> )	Stratification + Mixing	160	CH <sub>4</sub> µM = 9.9·10 <sup>-4</sup> CYA <sup>0.53</sup>	0.19	< 0.001
	Stratification	78	CH <sub>4</sub> µM = 1.7·10 <sup>-3</sup> CYA <sup>0.53</sup>	0.17	< 0.001
	Mixing	82	Not significantly related		0.666

994

995